Physics – Uspekhi **66** (1) 59 – 89 (2023)

REVIEWS OF TOPICAL PROBLEMS

PACS numbers: 07.20.Mc, 47.27.Cn, 47.32.C –, 67.25.dg, 67.25.dk

Quantum turbulence in superfluid helium

V B Efimov

DOI: https://doi.org/10.3367/UFNe.2021.11.039096

Contents

Abstract. **Helium at pressures below 25 atm remains liquid at temperatures down to absolute zero, when the number of excitations in the medium and the concentration of the normal component become negligible. This makes it possible to use superfluid helium at low temperatures as a model medium to study the formation and decay of a turbulent system. Describing and modeling the behavior of vortices in superfluid helium at temperatures below 0.1 K, when the amount of the normal component becomes negligible, are greatly simplified due to the quantization of the flow of the superfluid component, and all hydrodynamic properties of helium associated with its rotational motion are determined by quantized vortices. The article reviews experimental methods for the excitation and detection of quantum turbulence presented in experimental studies in recent years, and discusses features of vortex generation by various methods and at different temperatures of the superfluid, the dynamics of change in the concentration of vortices during the generation and decay of the vortex system, and the difference between the behavior of quantized vortices under Kolmogorov turbulence and that under Vinen turbulence.**

V B Efimov
Institute of Solid State Physics, Russian Academy of Sciences,
ul. Akademika Osip'yana 2, 142432 Chernogolovka, Moscow region,
Russian Federation
E-mail: efimov@issp.ac.ru

Received 2 July 2021, revised 17 October 2021
Uspekhi Fizicheskikh Nauk **193** (1) 63 – 95 (2023)
Translated by the author

Keywords: superfluidity, quantized vortices, turbulence, helium-4

1. Introduction

Turbulence is one of the most common natural phenomena occurring at lengths varying from nanometer (quantized vortex in a superfluid) to galactic scales (magnetic turbulence in the interstellar gas). It is an excited state of a system with many degrees of freedom, far from equilibrium. In fluid dynamics, turbulence is observed under certain conditions in the flow, when some characteristic scale parameter exceeds a critical value, e.g., when the dimensionless Reynolds number exceeds a few thousand, a turbulent state arises, leading to a disordered velocity of the flow particles and a chaotic change in the pressure in the liquid. In a turbulent state, all these parameters oscillate around the mean values. The Reynolds number is inversely proportional to the coefficient of kinematic viscosity (ν), and the experimental cell size for studying the behavior of a turbulent state can be reduced in size by decreasing ν. In this regard, experiments with liquid helium provide an opportunity to reduce the size of the experimental setup to study turbulent states by a couple of orders of magnitude in comparison with experiments with water or air.

If we talk about liquid helium (boiling point 4.2 K), when it cools below $T_\lambda = 2.17$ K under saturated vapor pressure, helium becomes superfluid, and it can flow without friction through narrow channels with sizes down to even nanoscale dimensions. However, the viscosity of flux of superfluid helium in bigger volumes is determined by the flow of the

normal component and the interaction of the normal and superfluid components, which will be discussed below. The coefficient of viscosity of air (at $T = 20\,^{\circ}\mathrm{C}$) is equal to $\nu = 0.01$ cm^2 s^{-1}, while, for gaseous helium ($T = 5.5$ K, 2.8 bar), $\nu = 3.21 \times 10^{-4}$ cm^2 s^{-1}, for helium I ($T = 2.25$ K, at the saturated vapor pressure), $\nu = 1.96 \times 10^{-4}$ cm^2 s^{-1}, and for superfluid helium in large volumes ($T = 1.8$ K, VSP), $\nu = 9 \times 10^{-5}$ cm^2 s^{-1} [1].

The main peculiarity of helium at temperatures below the phase transition ($T < T_\lambda$) is that it has two components, normal and superfluid, and this determines the fundamentally different behavior of helium in comparison with ordinary liquid. The superfluid component is a liquid in a quantum-correlated state, which manifests itself in such a phenomenon as the continuous flow of this component along closed lines and the existence of *quantized vortices*. For a large number of such disordered vortices in superfluid helium, their motion and the physical parameters of the medium (pressure, velocity of normal and superfluid components) can be complex and unpredictable, and for such motions only their average values are determined. A random tangle of such vortices is known as a turbulent state of *quantized vortices* and is called quantum turbulence. The term *quantum turbulence* was first introduced into the literature in 1986 by R J Donnelly [2] at a symposium dedicated to the memory of G I Taylor.

Hundreds of papers, both theoretical and experimental, are devoted to the study of the features of quantum turbulence. Let's focus attention on review publications [3–8]. Quite recently, a review of computational studies on the properties of vortex structure reconnections was published [9].

It is possible to compare the behavior of vortices in He-II at temperatures slightly below T_λ (due to the presence of both normal and superfluid components) and quantized vortices at temperatures near absolute zero, when the presence of the normal component and thermal excitations in liquid helium can be disregarded. The behavior of vortices at ultralow temperatures is the easiest kind for understanding and computer simulation due to the description of the quantized flows of the superfluid component around the vortices. However, in the region of intermediate temperatures, when the existence of vortices in both normal and superfluid liquids is possible, their interaction and energy transfer between them make the study of turbulence in helium very difficult.

In this review, we will consider turbulent processes in a system of quantum vortices in superfluid helium-4, mainly at low temperatures, the peculiarities of the formation of quantum turbulence, the conditions for the existence of an equilibrium concentration of quantum vortices during their steady generation, and the decay of a vortex system, we will analyze and discuss the results of recent experiments, and, finally, we discuss conclusions that were made on the basis of these experimental studies.

2. Turbulence in superfluid helium-4

The effect of superfluidity of liquid helium (He-II) was experimentally discovered by Kapitza as the ability of liquid helium at temperatures below 2.172 K to flow through micron-sized channels practically without any friction [10]. The coefficient of kinematic viscosity, a coefficient connecting the viscous force of friction when a fluid flows through narrow slots with the corresponding coefficients determined by the parameters of the slot, decreases during the transition of helium into a superfluid state by at least 6 orders of magnitude. This coefficient differs from the values of viscosity measured during the flow of superfluid helium through large channels or when helium moves in a large volume. The first experimental measurements of superfluid helium flux indicated the nonobservance of superfluidity; it was found in [11] that the experimentally observed 'critical velocities' at which superfluid hydrodynamics appear are significantly lower than the theoretical estimates obtained in Landau's theory of two-fluid hydrodynamics He-II [12, 13]. According to Landau's theory, violation of superfluidity occurs at flow velocities of the superfluid liquid V

$$V > \left(\frac{\mathrm{d}\varepsilon}{\mathrm{d}p}\right)_{p=p_0} \cong \frac{1}{m_\mathrm{r}}\left(\sqrt{2m_\mathrm{r}\Delta + p_0^2} - p_0\right) \sim 60 \text{ m s}^{-1},$$

where ε is the energy of quasiparticles in a liquid with momentum p, $m_\mathrm{r} = 0.16\, m_\mathrm{He}$ is the effective mass of the roton, $\Delta = 8.6$ K is the minimum energy of the roton and its minimum momentum $p_0 = 1.91$ Å^{-1}, while the measurements give the values of the velocities at which hydrodynamic friction appears, of the order of tens of cm s^{-1} [14–16]. The larger the channel size, the greater the viscosity calculated from the flow of superfluid helium through small-sized flow channels becomes. For a large channel (1 μm or more), the viscosity of superfluid helium approaches the viscosity of bulk helium.

The observed differences were explained within the framework of the two-fluid model of superfluidity, according to which helium-II consists of two interpenetrating liquids — the superfluid and the normal component. The superfluid component is helium, which is in a quantum-correlated state. One may define a macroscopic quantum fluid as a liquid with the wave function as [17]

$$\psi = \sqrt{\rho_\mathrm{s}}\exp\left(\mathrm{i}S(r,t)\right)$$

(order parameter), where r and t are a coordinate and time. The velocity of the superfluid component is defined as $V_\mathrm{s} = \left[\hbar/(m_{4\mathrm{He}})\right]\nabla S$. The superfluid component moves without friction, has zero entropy, and does not participate in the transfer of energy in the form of heat. The following property of superfluid helium is fundamental for quantum turbulence: the quantum-correlated state determines the long-range phase coherence of the superfluid component and imposes certain restrictions on the flow of the superfluid liquid V_s: when the phase S changes by $2\pi n$, where n is an integer, upon returning to the starting point observations, the wave function does not change, which determines the conservation of motion of the superfluid component at its circulation. In a simply connected region $\mathrm{rot}\, V_\mathrm{s} = 0$; however, for a multiply connected volume, the circulation of the superfluid component is quantized,

$$\Gamma = \oint_\mathrm{C} V_\mathrm{s}\,\mathrm{d}l = n\kappa,$$

where the integration is carried out along a closed line C. The multiple connectedness of the circulation volume can be realized by the presence in the volume of superfluid helium of a region with disturbed superfluidity — the size of a vortex with dimensions r_c being several angstroms for ^{4}He, $r_\mathrm{c} \approx 1.28 \pm 0.13$ Å at $T = 0.28$ K, and for ^{3}He-B, $r_\mathrm{c} \geqslant 100$ Å [18, 19]. The circulation quantum is defined as $\kappa = h/m_{4\mathrm{He}} = 9.998 \times 10^{-8}$ m^2 s^{-1}, where h is Planck's con-

stant, and m_{4He} is the mass of a helium atom. By quantized vortices we mean the region of superfluid flow around the core of the vortex, by direction of the vortex, the direction of its core, taking into account the direction of circulation of the superfluid component, and by density of vortices, the number of cores through a unit surface.

For a rectilinear vortex, the undamped velocity of motion of the superfluid component is defined as

$$V_s = \frac{\hbar n}{m_{4He} r} = \frac{\kappa n}{2\pi r},$$

where r is the distance from the vortex core. The quantum nature of the motion of the superfluid component around the vortex core was experimentally confirmed by research groups working on vibrating wires in superfluid helium [20, 21] and by experiments on the motion of negative charges connected with a vortex ring [22, 23]. The motion of the superfluid component around the core of the vortex determines the kinetic energy of a unit length of the vortex,

$$E_v = \int_{r_c}^{r} \pi \rho_s V_s^2 r \, dr = \frac{n^2 \rho_s \kappa^2}{4\pi} \ln\left(\frac{r}{r_c}\right),$$

where the integration is limited either by the size of the vessel for a single vortex or by the distance to the nearest neighboring vortices. It is energetically favorable for vortices to take the minimum possible n: a vortex with one circulation quantum $n = 1$ is stable in ^{4}He. For $n = \pm 1$, $\ln(l/r_c) \sim 10$ (which is quite reasonable for fairly highly dense packing of vortices), $\rho_s = 0.147$ g cm^{-3}, we obtain the energy per unit length of the vortex filament $E/L = (\rho\kappa^2/4\pi)\ln(l/r_c) \approx 1.2 \times 10^{-12}$ J m^{-1} $= 1.2 \times 10^{-18}$ J μm^{-1}.

Quantum turbulence is characterized by a large separation of size scales: the minimum scale is r_c — the size of the vortex core in ^{4}He $\sim 10^{-10}$ m, l is the average distance between the vortex lines (usually estimated as $l \approx \mathcal{L}^{-1/2} \sim 10^{-6}$ m, where $\mathcal{L}$ is the vortex density), and the largest scale is system size $D \sim 10^{-1}$ m.

By their nature (continuous flow of the superfluid component along the closed lines around the vortex core), quantized vortices in superfluid helium can begin and end on one of the vessel surfaces, including the liquid–vapor interface, or close on themselves in the form of vortex rings. An increase in the density of quantized vortices in superfluid helium is possible in several ways.

• First, an increase in the vortex densities occurs due to extension of the length of already existing vortex lines, which, bending under the action of a superfluid flow, intersect and reconnect with themselves or with neighboring vortices, and formats vortex loops [9, 24] (Fig. 1a–f). Numerical modeling within the framework of the nonlinear Schrödinger equation showed in [25] that reconnection occurs when the vortex cores are located at a distance of several interatomic distances.

• Second, nucleation of vortices is possible from the walls. To create a vortex from a wall, it is necessary to overcome the potential barrier, the value of which will be determined as $U_{max} \approx [\rho_s\kappa^2/(4\pi)][\ln(x/r_c) - 1]$ at a distance x_0 from the wall $\kappa/(4\pi V_c)$. This barrier can be overcome either thermally or by quantum tunneling, when the critical speed V_c is exceeded [26] (Fig. 1g). In helium II (except for temperatures close to T_λ), proper nucleation requires a sufficiently high velocity of superfluid component $V_H \approx 10$ m s^{-1}, which makes such a mechanism unlikely. An excess of VN and the nucleation of vortices of such a velocity is possible on sharp edges of vibrating bodies or upon ions motion in superfluid helium under the action of an electric field. The experimentally observed velocities of motion of oscillators in a superfluid liquid, at which a transition to turbulent vortex production occurs, have a significantly lower value of ~ 0.1 m s^{-1}, and the generation of vortices is associated with the first mechanism — an increase in the density of vortices from remanent vortices in the volume of the liquid and attached to the walls of the container and parts of a device.

Vortex lines can also be formed according to the Kibble–Zurek mechanism [27–29], when helium quickly jumps into a superfluid state from the normal state, for example, upon shock release of liquid pressure. In this case, the coherent wave function ψ can have a different phase in different regions of space and the vortex lines remain as linear defects separating the regions with a phase difference along a closed path $2\pi n$ [30].

The clearest method for the formation of ordered vortices is associated with the rotation with an angular velocity Ω of a vessel of radius R with superfluid helium. The total circulation of all vortices formed in it will be $\pi n_v R^2 \kappa$, and the equilibrium density of vortices in such a device will be $n_v = 2\Omega/\kappa$ [31]. The minimization of the energy of a vortex system in a rotating vessel forms a triangular structure of vortices (the Tkachenko vortex lattice [32], similar to the vortex structure of Abrikosov vortices of type-II super-

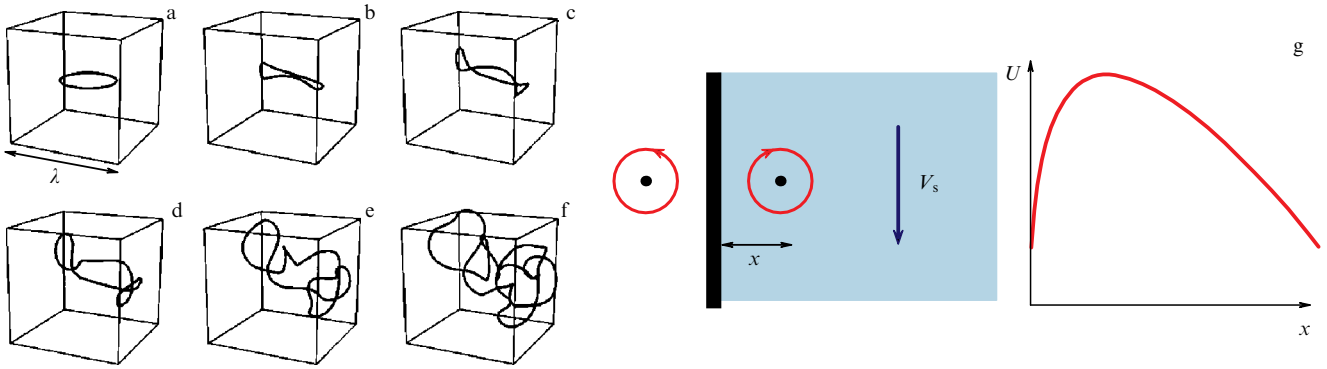

Figure 1. Calculation of time evolution of a vortex ring in the flow of a superfluid liquid in the direction of the diagonal of a cubic cell: conditional time from beginning of the experiment (a) $t = 0$, (b) $t = 1$, (c) $t = 2$, (d) $t = 3$, (e) $t = 4$, and (f) $t = 5$ (from [18]); (g) illustration of the nature of potential barrier during vortex nucleation from wall of the cell (from [26]).

conductors). In a superfluid vortex, along the direction of the core can exist a transverse wave excitation with a sound spectrum [33, 34], which was found experimentally [35–37].

When the vessel with superfluid helium stops rotating, an ordered system of unidirectional vortices turns into a vortex tangle, in which random processes decreasing the size of vortex rings occur due to reconnection, diffusion of small rings, etc. The process of reducing the density of vortices continues until their equilibrium value is established — the remanent vortex density. At a vessel rotation speed of one radian per second, such a 'spin-down' technique allows one to study the behavior of a vortex system with an initial vortex density of $\sim 10^3 - 10^4$ cm^{-2} [38] and the transformation of an ordered system of vortices into a turbulent system, and to study its decay with time, which is confirmed by model calculations [39].

One of the fundamental questions arising in the study of the motion of a superfluid liquid is the similarity and difference between quantum and classical turbulence. First, a quantized vortex has a quantized circulation of the superfluid component, and it differs from a vortex in a classical viscous fluid. Second, a quantized vortices is a vortex of a superfluid flow, and it cannot change the magnitude of the flow in an any closed loop or reduce the velocity of the superfluid component due to viscous friction, which is typical of a classical fluid. Such behavior of quantized vortices needs to have a special mechanism of energy dissipation of a system of vortices, especially in the absence of excitations in helium (at $T = 0$, really below 0.1 K). Third, the size of the core of the quantized vortex is of the order of the coherence length and for superfluid ^{4}He is only a few angstroms. Therefore, it is possible to determine with great accuracy the position of the quantized vortex in the liquid.

These properties make the behavior of a quantized vortex more definite than a classical one, which facilitates an accurate description and understanding of the behavior of quantum turbulence, the formation of a system of quantized vortices, its development in the process of interaction of vortices with each other, and its decay. In this respect, the most difficult behavior to describe is that of superfluid helium in the temperature range of 1.3–2.0 K. At these temperatures, along with the quantized flow of the superfluid component around the vortex core, there is a sufficiently high density of the viscous normal component, as well as mutual friction between the normal and superfluid components, which can act as a source and sink of energy for each of the components. For a two-component liquid, it is possible to create turbulence by mixing helium II using mechanical devices, for example, moving through the volume of superfluid helium a grid [40–42] or stirring the liquid with fan (a kind of 'washing machine' [43]). In this case, both the superfluid and the normal components of the liquid are turbulent.

The motion of the normal and superfluid components can be separated by locking the motion of the normal component. For this purpose, the entrance to and exit from the experimental volume are closed with plugs with small pores (superleak), through which the superfluid component can flow freely, while the motion of the normal component is inhibited by them. This type of turbulence, in which the normal component remains stationary according to the experimental conditions, or the concentration of the normal component becomes negligible with decreasing temperature, is called *one-component superfluid turbulence*. The behavior of a superfluid liquid at very low temperatures is of particular interest, since it refers to a simple and fundamentally important case when there are no complications associated with the motion of the normal component. Hereinafter, we will mainly consider quantum turbulence at very low temperatures.

The behavior of a classical viscous fluid is determined by the value of the dimensionless Reynolds parameter — the ratio of the velocity of the body relative to the fluid, the dimensions of the moving body, and the viscosity of the fluid. The enlarging of the Reynolds parameter over the critical value leads to a transition to the turbulent state. The behavior of superfluid turbulence is determined by two dimensionless parameters [44]. One of them is the internal parameter q, which characterizes the value of the friction force acting on the vortex relative to the nondissipative forces that determine the inertial motion of the vortex. The appearance of this parameter is associated with a description of the forces acting on a vortex in a superfluid liquid (an analogue of the Navier–Stokes equation for a classical viscous fluid, derived with averaging over scales larger than the characteristic distance between vortices), which determines the time evolution of vortex filaments for which $\mathbf{V} = \mathbf{V}_s$.

If we consider the processes only in a superfluid liquid and the motion of the normal component can be ignored, then we obtain the equation [45, 46]

$$\frac{\partial \mathbf{V}}{\partial t} + \nabla\mu = (1 - \alpha')\,\mathbf{V} \times \boldsymbol{\omega} + \alpha\,\hat{\boldsymbol{\omega}} \times (\boldsymbol{\omega} \times \mathbf{V})\,, \qquad (1)$$

where $\boldsymbol{\omega} = \nabla \times \mathbf{V}$ is the superfluid vorticity, $\hat{\boldsymbol{\omega}} = \boldsymbol{\omega}/\omega$, and the dimensionless parameters α' and α determine the reactive and dissipative forces acting on the vortex when it moves relative to the normal component. By introducing the notation $q = \alpha/(1 - \alpha')$, equation (1) can be written

$$\frac{\partial \mathbf{V}}{\partial \tilde{t}} + \nabla\tilde{\mu} = \mathbf{V} \times \boldsymbol{\omega} + q\,\hat{\boldsymbol{\omega}} \times (\boldsymbol{\omega} \times \mathbf{V})\,.$$

The first three terms define the inertial processes in classical hydrodynamics, and the fourth term with the parameter q determines the dissipation. For $q > 1$, the dissipative processes will dominate, and the flow of the superfluid component will be laminar; if $q \ll 1$, inertial processes will predominate, which makes possible the development of turbulence. Thus, the inverse parameter q^{-1} determines whether the flow of the superfluid component will be stable in case of its random deviation or the system can go into disordered motion (Fig. 2b). In classical hydrodynamics, developed turbulence described by the Kolmogorov spectrum is formed at $\mathrm{Re} \gg 1$. In a superfluid, developed turbulence can arise at $q \ll 1$.

The second parameter of superfluid turbulence, which determines the nature of turbulence, is the superfluid Reynolds number $\mathrm{Re}_s = VD/\kappa$, which contains the circulation quantum κ, which characterizes the quantized vorticity in superfluid.

Two parameters q and Re_s control the transition between two classes of superfluid turbulence. The first is the semiclassical regime, when energy transfer is formed similarly to the Kolmogorov cascade (modified by dissipation due to mutual friction of the normal and superfluid components and the possible transfer of energy between normal and superfluid vortices, state II). This type of turbulence of the superfluid component is characterized by a state where the vortices are locally polarized and vorticity quantization does not play a fundamentally important role for energy transfer in

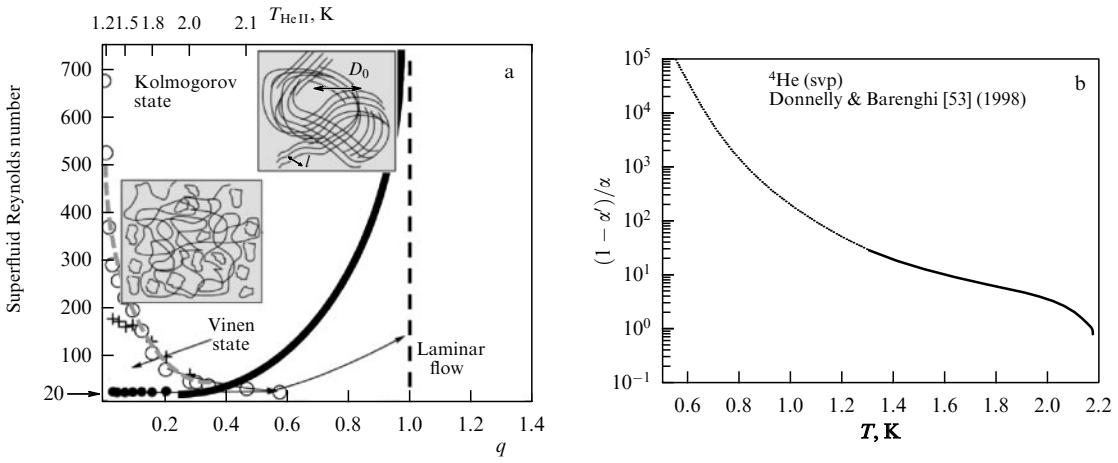

Figure 2. (a) One possible diagram of the dynamic states of vortices on the plane (Re_s, q) according to illustrations in [47, 48]. Symbols on the graph are the results of experimental work. Black dots — transition from state I to state II which was obtained in experiments with superlicks, when the motion of the normal component is inhibited [49]; circles [50] and crosses [51] — a similar transition in the case of counterflow of the normal and superfluid components. (b) Temperature dependence of q^{-1} showing the stability of the flow of the superfluid component at random deviations [53].

pulse space. The second type of turbulence is Vinen's quantum turbulence (state I), where the properties of the system are determined by the quantization of vorticity around individual vortices and the system of vortices is isotropic.

Kolmogorov turbulence, the energy spectrum of which has the form $E(k) \sim k^{-5/3}$, is located in the range of wave vectors $1/D \ll k \ll 1/l$, where D is the size of the system. In Kolmogorov turbulence, quantized vortices can move together with vortices in a normal fluid. Such turbulence can arise, for example, during intense mixing of superfluid helium ('washing machine' [43, 52]) at high temperatures (above 1 K). The turbulent Kolmogorov spectrum in this size range is also confirmed by model calculations [54]. The Kolmogorov type of turbulence is possible for one-component superfluid turbulence during the formation of *superfluid vortex bundles*, as shown in the inset in Fig. 2a, although we are not yet aware of experimental observations of such a behavior of vortices.

Vinen turbulence is characterized by a random vortex tangle with one dominant length scale l. The main experimental evidence for the existence of Vinen turbulence is that, if the vortex tangle decays, then the vortex line density decreases as $\mathcal{L} \sim t^{-1}$ [55, 56], which is consistent with the phenomenological Vinen model [57], which assumes a homogeneous and isotropic vortex configuration. The same decay $\mathcal{L} \sim t^{-1}$ was observed in numerical calculations [58], which also showed that the energy spectrum remains largely concentrated near $k \approx 1/l$.

A possible diagram of division into regions is shown in Fig. 2a. At a high flow rate $Re_s \gg 1$, the boundary of the behavior of a superfluid liquid between the turbulent and 'laminar' states approaches the vertical axis $q = q_0 \sim 1$. The line of demarcation of the two superfluid turbulence regimes arising at small q corresponds to the ratio $Re_s\, q^2 \approx 1$. The idea of such a demarcation lies in the conditions when, at a distance less than D_0, the detailing of the structure of individual vortices becomes unimportant and this corresponds to the condition $V_{s0} D_0 = q^2 V_s D = q^2 \kappa\, Re_s > \kappa$, or $Re_s > 1/q^2 \gg 1$. At high quantum Reynold's numbers, turbulence of the semiclassical type arises, which is characterized by a Kolmogorov-type cascade, possibly modified by mutual friction of the superfluid and normal components in He-II, which determines the transfer of energy between systems. Turbulence in this state becomes similar to that in classical fluids. At lower values of the Reynold's parameter, Vinen-type quantum turbulence develops. However, in contrast to classical fluids, the steady state of turbulence is determined not by viscosity but by the parameter of mutual friction q between the normal and superfluid components, and the energy losses of quantized vortices occur due to phonon emission at the motion vortex kink along the vortex core after reconnection (Kelvin waves, which will be discussed in Section 11).

Apparently, a division into two types of turbulence does exist, or at least such a picture of a rather abrupt transition between the laminar evolution of injected vortices and the emerging turbulent multi-vortex state of the entire superfluid liquid was observed at q of the order of unity for ^{3}He-B [59]. There is a similar behavior of superfluid ^{4}He at small q numbers: the existence of two different superfluid turbulences, in particular, is indicated by the fact that, at large Re_s numbers, the energy transfer in the inertial region of the frequency spectrum for both helium II and helium I are identical and correspond to the Kolmogorov spectrum $E(f) \sim f^{-5/3}$ (experiments with fast rotation of a fan in helium at $Re \sim 10^6$, $T = 2.3$ K, 2.08 K, and 1.4 K [43]).

3. Density of vortices — Vinen's quantum turbulence

The main characteristic of quantum turbulence is the density of vortices per unit area $\mathcal{L}$. For homogeneous turbulence, the direction of vortices is isotropic, although, for bunches of quantized vortices that can arise with intense mixing of a superfluid liquid and high quantum Reynolds numbers, one can determine the anisotropy and density of vortices, as well as the average vorticity of the liquid (as in Fig. 2a for the Kolmogorov type of superfluid turbulence).

Vinen first quantitatively described the dynamics of the density of vortex lines $\mathcal{L}(t)$ in the studies of 1957–1958 [57, 60–62] based on experimental data. For a uniform density of vortices $\mathcal{L}$, the distance between vortices is $l = \mathcal{L}^{-1/2}$. The

density of vortices is determined by two processes: the rate of generation of vortices and the rate of their decay. If the process of vortex generation is determined by the velocity of the superfluid component, its gradients, and the value of the counterflow of the normal and superfluid components in the presence of heat fluxes, i.e., external influences on a superfluid liquid, the decay process is determined by a change in the shape of moving vortex rings, cascade fragmentation of vortex rings when they intersect with themselves or neighbors in a turbulent system (reconnection processes), a decrease in the size of vortex loops due to interaction with the normal component, radiation energy by Kelvin waves as a motion of kinks along the vortex core, and finally, the diffusion of vortices from the place of their generation and their disappearance on the walls of the vessel.

The ratio of these two processes (generation and annihilation) will determine the temporal dynamics of the density of vortices

$$\frac{\mathrm{d}\mathcal{L}}{\mathrm{d}t} = \left[\frac{\mathrm{d}\mathcal{L}}{\mathrm{d}t}\right]_{\mathrm{g}} - \left[\frac{\mathrm{d}\mathcal{L}}{\mathrm{d}t}\right]_{\mathrm{a}}.$$

Vinen measured the density of vortices by the attenuation of second sound waves, using the counterflow of the normal and superfluid components during local heat emission as a vortex generator, which determined the operating temperature range above 1.3 K. In the phenomenological theory of quantum turbulence, Vinen proceeded from the locality of the change in the vortex density, that interaction forces act on the vortices, determined in some form from the distance between the vortices, the interaction forces of the normal and superfluid components of $\mathbf{V}_{\mathrm{ns}} = \mathbf{V}_{\mathrm{n}} - \mathbf{V}_{\mathrm{s}}$. A dimensional analysis and the experimental fact of the growth of the vortex ring radius that is proportional to the acting force [63] allow us to conclude that the density of vortices in the vortex coil grows as

$$\left[\frac{\mathrm{d}\mathcal{L}}{\mathrm{d}t}\right]_{\mathrm{g}} = \alpha_{\mathrm{V}}|\mathbf{V}_{\mathrm{ns}}|\mathcal{L}^{3/2}, \tag{2}$$

where $\alpha_{\mathrm{V}} \sim C\alpha$, with a constant C of the order of unity, determined from the experiment.

To determine the decay rate of the vortex structure, Vinen suggested a mechanism analogous to classical isotropic turbulence, which implies the existence of an inertial interval of energy transfer from the pumping region to the dissipative region at large wave numbers. In the theory of homogeneous isotropic turbulence, the energy dissipation associated with inertial energy transfer is described as [64]

$$\left(\frac{\partial u^2}{\partial t}\right)_{\mathrm{a}} \propto -\frac{u^3}{l_{\mathrm{visc}}},$$

where u is the characteristic velocity on the scale l_{visc}, corresponding to the viscous limit of the inertial interval. If we take as l_{visc} the distance between the vortices $l = \mathcal{L}^{-1/2}$, and as the velocity u the velocity of the superfluid component at a distance l from the vortex core as $V = \kappa/(2\pi l) = (\kappa/2\pi)\mathcal{L}^{1/2}$, then, as a result, the vortex decay rate can be written as

$$\left[\frac{\mathrm{d}\mathcal{L}}{\mathrm{d}t}\right]_{\mathrm{a}} = \beta_{\mathrm{V}}\mathcal{L}^2,$$

where β_{V} is a parameter close in order of magnitude to $\kappa/(2\pi)$. A similar dependence is obtained when we consider the probability of dissipative processes in a vortex system arising due to reconnection and the decrease in the size of vortices associated with this process. The probability of a reconnection for each vortex will be proportional to the density of the vortices. If we are interested in energy losses in a system of vortices, i.e., the rate of decrease in the total length of the vortices during the interaction of all vortices with each other, then we obtain the value $\sim \mathcal{L}^2$. As a result, the change in the density of vortices in space with a uniform and isotropic distribution of vortices will be written as follows:

$$\frac{\mathrm{d}\mathcal{L}}{\mathrm{d}t} = \alpha_{\mathrm{V}}|\mathbf{V}_{\mathrm{ns}}|\mathcal{L}^{3/2} - \beta_{\mathrm{V}}\mathcal{L}^2. \tag{3}$$

This relation is called Vinen's equation.

Vinen's equation makes it possible to estimate the average density of vortices under stationary conditions, when $\mathrm{d}\mathcal{L}/\mathrm{d}t = 0$. It is not difficult to see that the equilibrium density of vortices will arise at a constant heat flux, when there is a counterflow of the normal and superfluid components of the $\mathbf{V}_{\mathrm{ns}}$. Experiments with the generation of vortices by a heat flux are carried out at temperatures where the density of the normal component cannot be ignored, i.e., at temperatures $T > 1$ K.

The condition for the applicability of Vinen's equation is the need for the existence of *remanent vortices* (so-called remanent vorticity) in the volume of liquid helium to increase their density during heat fluxes (Fig. 1a–f). If at the beginning of the experiment or after the collapse of the vortex system after the heat flux is turned off the density of vortices is equal to 0, then no vortices will arise for any value of $\mathbf{V}_{\mathrm{ns}}$. Such a picture is observed when smooth filaments oscillate, if they do not have pinning vortices, for which even high speeds of their movement do not lead to a transition to a turbulent state in the system. The possibility of vortex nucleation from the vessel walls was discussed earlier (Fig. 1g).

We point out that, almost always, despite all the precautions in preparing the experiment with superfluid helium, there are remanent vortices in the liquid, which are pinned on all surfaces. In Figure 3, shown is the temporal change in the quality factor of a quartz tuning fork, the value of which depends on the pinning of vortices (as an added

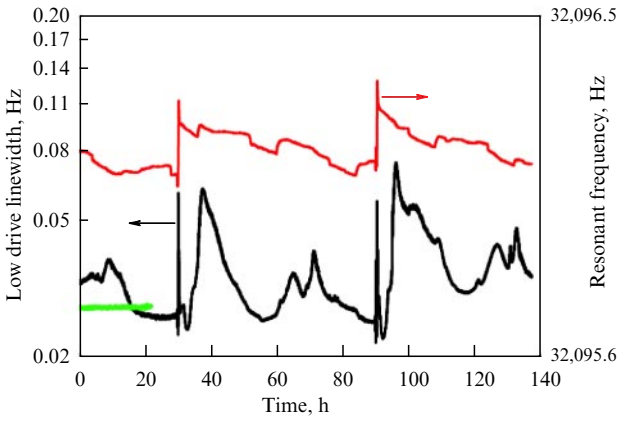

Figure 3. Time dependence of the quality factor of a quartz tuning fork and its resonant frequencies in superfluid helium-4 at temperature $T = 10$ mK. At times of 30 and 90 hours, liquid helium was poured into the cryostat. (From [65].)

mass) at a low temperature [65]. It is clearly seen that the quality factor of the tuning fork varies over a fairly wide range, as does its resonant frequency. We will consider in more detail the possibility of quartz tuning forks to detect vortices in Section 14.

To test the proposed phenomenological theory, Vinen measured the scattering of second sound waves as a function of time in two channels with cross sections of 2.4×6.45 mm^2 and 4.00×7.83 mm^2 and a length of 20 cm at temperatures from 1.3 K to T_λ at various intensities of heat flux. These measurements were the basis of the proposed theory, although other relations are possible for the growth of $\mathcal{L}$ when the vortex flow is turned on, in particular, relation (2) may look like $[\mathrm{d}\mathcal{L}/\mathrm{d}t]_\mathrm{g} = \alpha_\mathrm{F}|\mathbf{V}_\mathrm{ns}|^2\mathcal{L}$, which is somewhat in disagreement with the experimental data. This relation corresponds to the case when the influence of vortices on each other is neglected and only $\mathbf{V}_\mathrm{ns}$ is dominant in the Magnus effect, which is responsible for the increase in the length of the vortex.

From Vinen's equation, one can determine the stationary concentration of vortices at a constant heat flux:

$$\mathcal{L}_\mathrm{st} = \frac{\alpha_\mathrm{V}^2}{\beta_\mathrm{V}^2}\,\mathbf{V}_\mathrm{ns}^2 = \gamma^2\,\mathbf{V}_\mathrm{ns}^2\,. \tag{4}$$

Vinen's equation makes it possible to estimate the time of formation of a vortex tangle τ_V. Integration of relation (3) gives the divergence in time to reach the value of $\mathcal{L}_\mathrm{st}$; therefore, to estimate τ_V, it is possible to determine the time of creation of the vortex density $\mathcal{L} = \mathcal{L}_\mathrm{st}/2$:

$$\tau_\mathrm{V} = c_v(T)\dot{q}^{-3/2}\,. \tag{5}$$

4. Generation of quantum turbulence by heat flows. Interaction of second sound waves with a vortex structure

For temperatures above 1 K, when there is a significant amount of the normal component, the absorption of second sound waves is used as one of the main methods of detection of quantum turbulence. The features of second sound propagation in superfluid helium-4 have been studied in detail and described in many papers (for example, in [1, 66–68]). Here, we shall review the interaction of second sound waves with vortices and the generation of a vortex tangle by heat fluxes in He-II.

Experimental studies of the propagation of second sound waves in rotating containers (with angular velocity $\mathbf{\Omega}$) have shown a dependence of the signal attenuation with respect to angle θ (between the direction of the vortices aligned along the axis of rotation and the direction of propagation of sound waves) [69, 70]. One can write the mutual friction force $\mathbf{F}_\mathrm{ns}$ between the normal and superfluid components as

$$\mathbf{F}_\mathrm{ns} = -\alpha\kappa\frac{\rho_\mathrm{s}\,\rho_\mathrm{n}}{\rho}\mathcal{L}(\mathbf{V}_\mathrm{n} - \mathbf{V}_\mathrm{s})\sin^2\theta\,,$$

taking into consideration the total rotation of single vortices in the container $\mathbf{\Omega} = 1/2\,\kappa\mathcal{L}\hat{\boldsymbol{\omega}}$. The attenuation of the second sound waves, proportional to the value of $\mathbf{F}_\mathrm{ns}$, will be proportional to the vortex density $\mathcal{L}$ and for homogeneous quantum turbulence $\langle\sin^2\theta\rangle = 2/3$. There are two limiting cases: when $\sin^2\theta = 0$ for the parallel direction of the vortex axis and the propagation of the second sound and $\sin^2\theta = 1$ in the perpendicular direction.

Superconducting bolometers [71] are used as a detector of *second sound waves*; the transition temperature of the superconductor depends upon the material of the film, and it can be shifted to lower temperatures by applying a magnetic field. Sensors based on membranes with small pores (~ 100 nm) [72] are also used as receivers. The membrane sensor action is based on the ability of the superfluid component to flow through small pores, while the viscous normal component cannot go through. As a result, the pressure inside the sensor changes in accordance with the change in the amount of the superfluid component (and the temperature in the measured wave). Both sensors have their own advantages and disadvantages.

Heaters of various types are usually used as a source of *second sound waves*, such as film resistances, as can porous membranes for the detector.

Two methods are used to measure the absorption of *second sound waves — pulsed and resonant*. The resonant technique has a higher sensitivity, but is limited by its temporal resolution, which is determined by the quality factor Q of the system; a high Q slows down the system response upon a change in absorption along the path of second sound waves. The pulse technique has a higher temporal and spatial resolution but has a lower sensitivity. The technique for measuring the absorption of second sound waves usually uses wave propagation in the direction perpendicular to the source of turbulence. For example, the change in the resonant characteristics of standing waves of the second sound is measured in the direction of a perpendicularly elongated ampoule, along the long side of which a fine mesh is stretched at high speed [41] or a constant heat flow is turned on [72, 73]. In the first case, the absorption of the second sound allows the decay processes of a vortex system associated with both the superfluid component and the normal one to be investigated. In the second scheme of the setup, it is possible to study the formation of quantum turbulence, its stationary characteristics, and its decay, i.e., to investigate its temporal parameters and dependences on the magnitude of heat fluxes.

Interaction of vortices and ions in liquid helium. Another way to study quantum turbulence over the entire temperature range is to study the propagation of charged particles in superfluid helium. The motion of positive helium ions (He^+) creates a compaction zone of helium atoms, forming a nano-solid-helium aggregate consisting of about 20 helium atoms ('Ferrell's snowball model' [74]), while the motion of negative charged particle such as electrons forms a nanosized bubble due to quantum mechanical repulsion of the environment by a light particle (electron) — 'Atkin's bubble model' [75]. Such a bubble in liquid helium has a rather large hydrodynamic added mass of about 200 helium atoms. The motion of both kinds of ions can be controlled by an externally applied electric field and is affected by the presence of quantized vortices. Due to the pressure gradient of the superfluid circulation around the vortex, there is an attractive interaction between ions and vortices that can capture ions by the vortex cores.

Generation of vortex turbulence by heat flows. Experimental studies of counterflow turbulence in He-II began with experiments on heat transfer through channels of different sizes. The heat flow in He-II is characterized by the counterflow of the normal and superfluid components and has no obvious counterpart in flows of a classical ordinary viscous liquid. If one tries to find a possible connection

between thermal backflow and classical turbulence, thermal convectional turbulence is a likely candidate.

The heat flux with density $\dot{q}$ emitted by the heater at one end of the channel is carried away only by the normal liquid, while, because of mass conservation, the superfluid component moves in the opposite direction. Thus, a counterflow occurs along the channel with velocity $\mathbf{V}_{ns} = \mathbf{V}_n - \mathbf{V}_s$. The velocity of the normal liquid is $\mathbf{V}_n = \dot{q}/(ST\rho)$, where S is the specific entropy of He-II, assuming that $\dot{q}$ is fully used to transform the superfluid component into a normal liquid. The velocity of the superfluid component $\mathbf{V}_s$ is calculated from the condition $\rho_n \mathbf{V}_n + \rho_s \mathbf{V}_s = 0$. At relatively small values of $\mathbf{V}_{ns}$, the flow remains laminar. An increase in eddy turbulence and an increase in the number of eddies begins at a certain heat flux density, the value of which can be determined experimentally. One of the methods for determining the transition to quantum turbulence was implemented by visualizing the motion of counterflow with the help of optically excited helium atoms and, consequently, observing the time-dependent position of moving excited atoms [76]. In the temperature range of 1.6–1.8 K and at a constant heat flux $\dot{q} < 30$–$50\ \text{cm}^{-2}$, the counterflow remains laminar. Exceeding the indicated values of the heat flux leads to the appearance of a turbulent state of superfluid helium, which is characterized by its disordered flow, and the behavior of the luminous path changes when the flux density exceeds 60–65 mW cm^{-2} [77]. Similar values of the heat flux, which do not transfer the fluid into a turbulent state, were obtained in [78], where the vortex state was tested by measuring the temperature gradient.

The phenomenological theory of vortex generation by a heat flux has been considered in detail in reference [79]. In brief, for a weak heat flux, the mutual friction F_{ns} and the term $\mathrm{d}V/\mathrm{d}t$, which determines the acceleration of the motion of the corresponding component, are equal to zero, based on the continuity equations for superfluid helium and taking into account that the heat flux through superfluid helium is defined as the motion of a normal component. This assumption leads to the following equation of state for liquid helium:

$$\nabla p = \rho S \nabla T ,$$

a relation known as the London equation. The pressure gradient caused by a laminar Poiseuille flow of the normal component is defined as

$$\nabla p = \eta \nabla^2 V_n ,$$

where η is the viscosity of the normal component. When a laminar heat flow streams along a tube with diameter d, the pressure difference is

$$\nabla p = \frac{32 \eta V_n}{d^2} ,$$

and we obtain for the laminar heat flow in a long pipe

$$\nabla T = \frac{32 \eta}{\rho^2 S^2 T d^2} \dot{q} .$$

At high heat fluxes, as we noted above at $\dot{q} > 30$–$50\ \text{mW cm}^{-2}$, mutual friction occurs, which is determined by an increase in the number of vortices, and quantum turbulence is formed. In this case, the mutual friction term F_{ns} turns out to be dominant in the Navier–Stokes equations for the normal and superfluid components. This quantity was defined in [80] as

$$F_{ns} = A_{GM} \rho_s \rho_n |\mathbf{V}_s - \mathbf{V}_n|^3 , \tag{6}$$

where the A_{GM} coefficient is called the Gorter–Mellink constant. If we assume that the mutual friction of the normal and superfluid components is dominant in the Navier–Stokes equation at high heat fluxes with developed quantum turbulence, then the temperature gradient is defined as

$$\nabla T = \frac{F_{ns}}{\rho_s S} .$$

As a result, we get

$$\nabla T = \frac{A_{GM} \rho_n}{S} \left(\frac{\dot{q}}{\rho_s S T} \right)^3 .$$

Equation (6) was further modified by Schwartz [81] to include a small velocity shift $\mathbf{V}_0$, which is associated with the beginning of the formation of turbulence in the vortex system, considering the Vinen equation. So, the final equation has the form

$$F_{ns} = \mathcal{L}_{st} f = A_{GM} \rho_s \rho_n (\mathbf{V}_n - \mathbf{V}_s - \mathbf{V}_0)^2 |\mathbf{V}_n - \mathbf{V}_s| .$$

A_{GM} is calculated from experiments on the appearance of a temperature gradient at heat flows that form fully-developed turbulence, and it has a temperature dependence of the form $A_{GM} \sim T^3$ (Fig. 4).

The formation of a turbulent state requires time to increase the density of the vortex tangle in the counterflow that occurs during heat emission, so the transition to turbulence for heat pulses occurs at significantly higher heat flux densities. In measurements of double thermal pulses with a duration of 10 μs, the transition to an increase in the absorption of the second pulse occurs: $\dot{q} \sim 10-15\ \text{W cm}^{-2}$. The decrease in the second heat pulse means that it traveled through the medium, where the density of vortices had

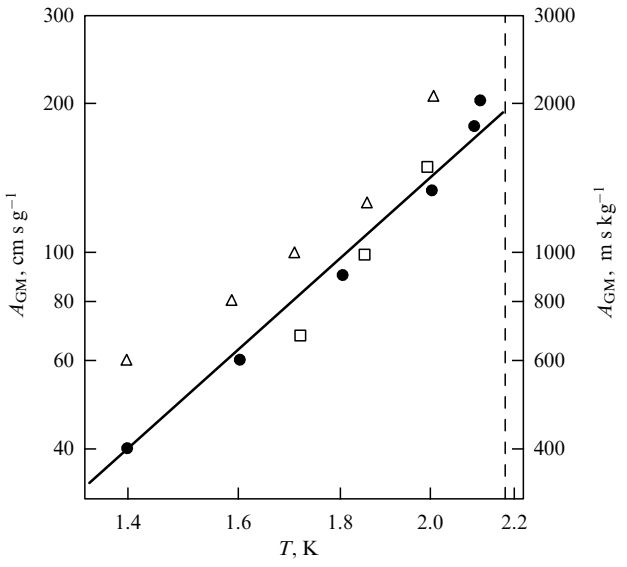

Figure 4. Temperature dependence of the Gorter–Mellink constant A_{GM}. Taken from results of [57, 79, 82, 83].

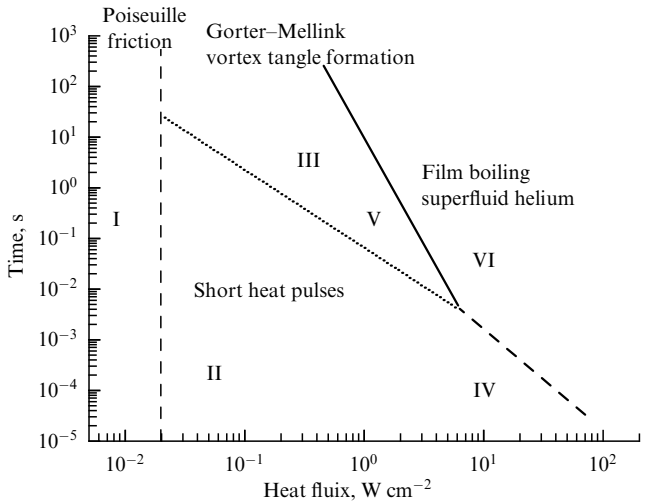

Figure 5. Experimental data on the influence of a thermal pulse on the behavior of superfluid helium, depending on heat flux density and single pulse duration. In region III, the vortex tangle is formed due to friction of the normal and superfluid components — the Gorter–Mellink interaction (from [86]).

already begun to increase. The increase in the vortex density is proportional to time [84]:

$$\frac{d\mathcal{L}}{dt} \approx \gamma \left(\frac{\dot{q}}{\rho S T} \right)^{5/2} t .$$

The power at which the density of vortices began to increase significantly decreased when the successive launches of double signals were a few milliseconds shorter. During the times between launches, the density of residual vortices remained sufficiently high. In [85], a cooling pulse was used as a test signal after a heating one. Positive–negative temperature pulses appear during the propagation of a long thermal pulse in the three-dimensional geometry.

An approximate division of the state of superfluid helium depending on the duration of a single pulse under the effect of a heat flux is shown in Fig. 5. The scheme can be conditionally divided into six regions of heat flux influence on superfluid helium, depending on their temporal impact. I — laminar Poiseuille counterflow of normal and superfluid components in the region of constant heat fluxes $\dot{q} < 30-50$ mW cm^{-2}; II — short thermal pulses, where the heat flow propagates with the second sound speed, and the vortex system does not have time to develop; III — region of heat transfer with vortex multiplication, with quasi-classical turbulence formed due to friction of the normal and superfluid components, and the line of separation of regions II and III is approximately described by relation (5): $\tau_V = c_v(T)\dot{q}^{-3/2}$, where coefficient $c_v(T) \approx 0.1$ W$^{3/2}$ s cm^{-3} (and depends on temperature [87]); IV — conditional region where pulses begin to generate a fully developed turbulent state [84]; V — fairly dense vortex tangle formed near the heater, which decelerates the normal component; this process leads to a local transition of superfluid helium to the normal state, followed by boiling [88]; VI — film boiling of helium on a heater [89], where the time of simmer at pulsed heating t_{boil} is described by the relation $\dot{q} t_{boil}^{1/2} = C$, where $C \sim 0.05-0.5$ W cm^{-2} s$^{1/2}$.

It is worth recalling that the above diagram is conditional and shows only trends in the formation of the state of superfluid helium under different temporal-thermal actions, and the actual behavior can differ greatly depending on the geometry of the experiment. For example, at a constant heat flux of 50 mW cm^{-2}, a uniform density of vortices should be established in the entire sample volume over times of the order of ~ 10 s. However, in experimental investigations of the distribution of the temperature gradient in a long capillary at a constant heat flux [90] that was enough for the development of the turbulent state in a capillary ($D_{in} = 1.4$ mm, $L = 8.0$ m, $\dot{q} = 44-60$ mW cm^{-2}, $T = 1.34$ K), the settling time was two orders of magnitude longer, while the vortex tangles moved both from the side of the heater and from the open part of the capillary with velocities of 1–3.7 and 0.1–2.5 mm s^{-1}, respectively. This experiment confirms the necessity for a remnant vortex density to generate quantum turbulence upon its formation by a counterflow of the normal and superfluid components.

The technique of forming a vortex structure by counterflow of the normal and superfluid components makes it possible to use the attenuation of second sound waves as a detector of the vortex structure. The temperatures at which such studies are possible lie above 1 K, where the density of the normal component is still high. However, in this temperature range, turbulence can be established in both normal and superfluid systems, which interact together through mutual friction. In order to interpret the experimental data, it is necessary to take into account the deceleration of the normal component near the channel walls, which causes distortion of the flat profile of the counterflow $\mathbf{V}_{ns}$ and becomes significant in experiments in thin channels. In general, vortex generation by a heat flow is characterized by the first term in Vinen equation (3) and depends on the resistive interaction constant α and on the value of the counterflow.

Experiments on the study of the vortex distribution in a wide channel (rectangular section of 1×2.3 cm^2) [91] with the help of negative ions during their formation by the counterflow determined that the density of vortices over the channel cross section is uniform and the normal liquid flow profile is flat, except the viscous flow region near the walls (~ 1 mm), with an accuracy of several percent.

Measurements of the temperature gradient along a channel with a counterflow of the normal and superfluid components [92] showed that there are several stable turbulent states, depending on the geometry of the experimental cell. In rather large round or square channels, the laminar flow undergoes the first transition at heat flux $\dot{q}_{c1}$, above which the measured ΔT only slightly exceeds the extrapolated laminar value. At $\dot{q}_{c2}$, the second transition occurs, above which the measured ΔT increases sharply. These turbulent states are referred to as TI and TII (Fig. 6).

The possibility of the existence of the TI state under conditions when $\dot{q}_{c1} < \dot{q} < \dot{q}_{c2}$ was noted in work on the attenuation of second sound waves [57, 60–62], as well as in experiments on measuring the pressure difference [93] and temperature difference [51, 78] upon passage of a constant heat flux.

The Biot–Savart law is usually used in full or local form to model and calculate the behavior of vortex filaments. The Biot–Savart law takes into account the motion of a liquid (superfluid component) around the vortex core and the effect of this motion on other vortices. The full Bio–Savart law considers the influence of all volume elements on a given segment of the vortex. The approach requires a rather large number of calculations. Often, the local Biot–Savart law is

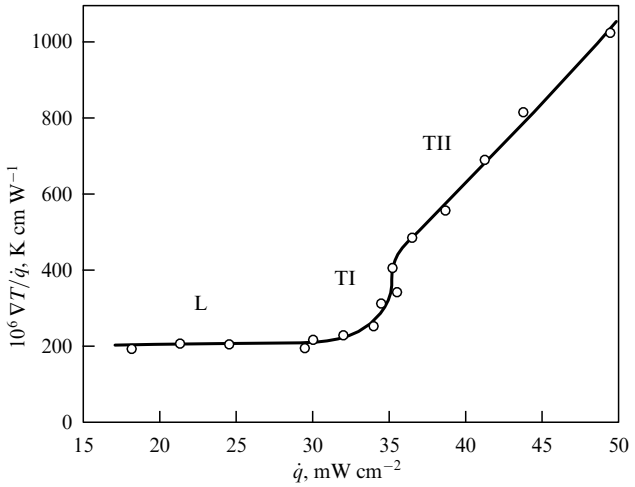

Figure 6. Thermal resistance ($\nabla T/\dot{q}$) as a function of heat flux density at $T = 1.15$ K [92].

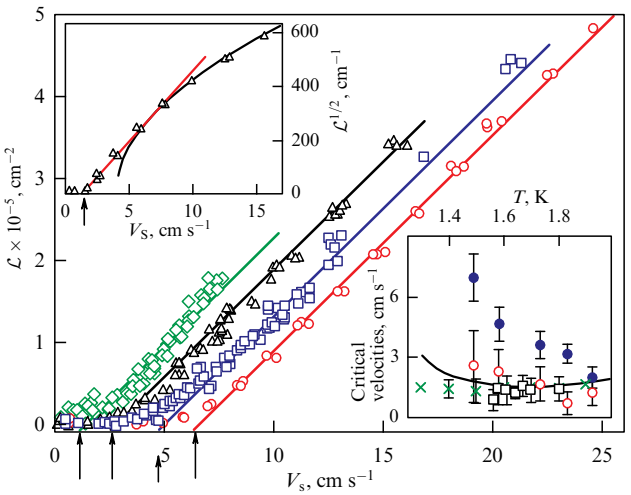

Figure 7. Steady-state vortex line density versus mean superfluid velocity in a channel. Center graph shows dependences of vortex density on the speed of the superfluid component at different temperatures; solid lines correspond to dependences $\mathcal{L} = \beta(V - V_{cr}^{TII})$, where $\beta = 2.65 \times 10^4$ cm^{-3}: data at $T = 1.92$ K (green diamonds), $T = 1.73$ K (black triangles), $T = 1.58$ K (blue squares), $T = 1.49$ K (red circles); blue arrows from below indicate $\mathcal{L}^1 \sim V_s$ (TII). Top-left inset shows data on the distance between the vortices as a function of the speed of the superfluid component; thick red line is the $\mathcal{L}^{1/2} \sim V_s$ (TI) dependence, black line is $\mathcal{L}^1 \sim V_s$ (TII), $T = 1.73$ K. Lower-right inset shows dependences of the V_{cr}^{TI} temperature (blue dots), black squares plot the values of V_{cr}^{TI} rates for the 10-mm channel, red circles are V_{cr}^{TI} for 6-mm channel. Green crosses X's show data and solid line is the prediction of the theory (taken from [96]).

used to model the behavior of vortices, taking into account only the influence of the nearest segments of the vortex line based on considerations that the closest segments of the vortex line have the greatest effect on the dynamics of the vortex point, i.e., in calculations, they are limited to sections of the vortex filament. This significantly weakens computing power requirements. Considering the transition of the system to a turbulent state, it was shown in [94] that the simulation of a vortex filament in a steady counterflow turbulence using the full Biot–Savart law gives isotropic turbulence, while calculations in the local approximation create a layered structure of vortices that does not transition into an isotropic turbulent state. Since agreement between the experimental data and the theory of homogeneous isotropic turbulence is worse at TI than at TII (for which this theory works quite well), the state of TI can be inhomogeneous and not isotropic. This behavior is associated with a low density of generated vortices. The low density of vortices at TI sharply reduces the influence of superfluid flows from distant vortices and increases the influence from nearby parts of the vortex.

As experiments have shown, the geometry has a strong influence on the turbulence generated by the counterflow. In rectangular channels with a big aspect ratio (1:10) and a small size of less than 100 μm, only one transition was observed at $\dot{q}_{c3}$, denoted in contrast to the previous transitions as TIII [91].

The existence of two clearly distinguishable stable turbulent states in the 'counterflow' turbulence of He II, as well as the existence of the TIII transition in small channels, has been a mystery for a long time. One possible explanation was proposed in [95], where it is assumed that the superfluid is turbulent in the TI state, but the normal fluid is still laminar. Thus, the transition from TI to TII may correspond to the onset of the transition of the normal component of helium II to the turbulent state. However, a similar behavior of the transition from a laminar flow to a developed turbulence through a certain intermediate state was also observed at ultralow temperatures, when the turbulence of the normal component cannot exist in principle. An alternative interpretation will be discussed in Sections 9, 10, 13, and 14.

The complexity of interpreting the results of experiments with the generation of turbulence by heat fluxes is associated precisely with the presence of two components that interact with each other, and turbulence can arise both in the superfluid and in the normal component.

In the experiments described in [96], the motion of the normal component was suppressed by creating a flow of only the superfluid component through two porous plugs (superleaks) using the fountain effect. However, taking into account the mutual friction of the normal and superfluid components, some toroidal flow of the normal component still remains in this setup of the experiment. The results of the measuring concentration of vortices by the attenuation of second sound waves in a directed flow of only the superfluid component are shown in Fig. 7. The graphs in Fig. 7 (upper-left inset) clearly show the change in the regime of vortex generation with an increase in the flow velocity of the superfluid component: we call this transition from laminar flow (L) to turbulent flow (TII), in accordance with the results presented above, TI. An intermediate region of the velocities is also observed in the transition from laminar motion to the regime of developed quantum turbulence in experiments where the generation of turbulence takes place via the motion of oscillating bodies in superfluid helium at low temperatures.

The results of investigations of vortex generation using heat fluxes are difficult to interpret due to the movement of both the normal and superfluid components, the possibility of the existence of turbulent states in both systems, their mutual friction, and energy transfer between them. The situation is simplified when the superfluid liquid is cooled to temperatures below 0.1 K, where the concentration of the normal component can be ignored. However, the 'counterflow' regime of turbulence generation under such conditions is impossible, and other methods are used to create vortices, in particular, oscillations of various kinds of solids in a superfluid liquid.

5. Generation of turbulence by moving bodies

The use of the motion of bodies or fluids around bodies immersed in fluids to generate turbulence has a long history dating back to the observations of Leonardo da Vinci, whose drawings of vortices in water demonstrate perhaps some of the first documented interest in turbulence. One of the methods in experimental fluid dynamics for the inception, growth, and decay of turbulence in fluids, both classical and superfluid helium, has been the observation of the change in the quality factor of oscillating bodies in a medium under resonant conditions. We would like to mention the recent reviews by Vinen and Skrbek [97, 98] that analyze the possibilities of generating turbulence using oscillating systems.

When a solid body moves in a liquid, the resistive drag experienced by it depends upon the cross section of the body A_s, its speed V, the viscosity of the liquid, and its density. The value of the drag force depends on the drag coefficient C_d, which is determined by the conditions of fluid flow around the body under circumstances of turbulent flow:

$$F = \frac{1}{2} C_d \rho A_s V^2 = \gamma V^2 . \tag{7}$$

In classical fluids, the turbulent coefficient C_d^T at high velocities depends on the shape of the body and is approximately constant c_T, of the order of unity. The drag coefficient is defined as $\gamma = C_d^T \rho \pi R^2/2$ for a sphere, e.g., $C_d^T = c_T \approx 0.4$.

At low velocities, when the flow is laminar, a dissipative drag arises from the viscosity of the fluid and is known as the Stokes drag. The drag coefficient C_d^L for an object oscillating with a frequency $f = \omega/(2\pi)$ is given by the expression $C_d^L = c_L \sqrt{\omega\nu}/V$, where ν is the kinematic viscosity and c_L is a geometric constant of the order of unity. This relationship is valid when the penetration depth $\delta = \sqrt{2\nu/\omega}$ of the viscous fluid flow is small compared to the size of the object. The ratio of the object size to the penetration depth determines the Stokes number $\beta_S = fd^2/\nu \approx (d/\delta)^2$. The Stokes number is much greater than 1 for typical objects with dimensions of several millimeters moving in normal helium $\beta_S \gg 1$. For a laminar flow, the drag force (7) will be proportional to the speed of movement.

The turbulent drag will be equal to the Stokes drag at speed

$$V_x \cong \frac{c_L}{c_T} \sqrt{\omega\nu} . \tag{8}$$

Characteristic drag coefficients for bodies of various shapes are shown in Fig. 8. The drag coefficient C_d becomes about unity at Reynolds numbers $\mathrm{Re} \approx 10^2 - 10^3$.

In a classical fluid, however, oscillating objects usually do not have a well-defined critical velocity above which the flow becomes turbulent: the flow becomes more complex as it transforms from low-velocity laminar to higher-velocity turbulence. Often, there is a wide transition region with many completely different flow regimes, while the drag coefficient C_d changes smoothly with an increase in speed [99, 100].

To characterize the motion of a body in a fluid, in particular at resonant oscillations, the Keulegan–Carpenter number (KC) is determined as a dimensionless quantity that characterizes the ratio of the drag force to the inertia forces for oscillating bodies in a fluid at rest: $\mathrm{KC} = 2\pi A/d$, where A is the relative motion amplitude and d is the size of the moving

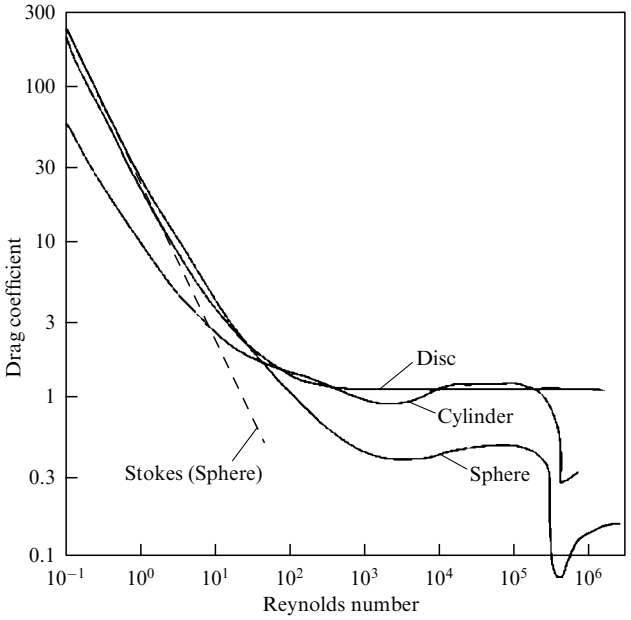

Figure 8. Graph of the dependence of the drag coefficient on the value of the Reynolds number for a disc, cylinder, and sphere. Dotted line shows the Stokes relation for a sphere in a laminar flow [101].

object, such as the diameter of a cylinder. A small KC number means that the inertia forces dominate, while a large number means that the (turbulent) drag forces prevail. In classical liquids, the picture of the formation of a turbulent structure varies, depending on the Stokes and Keulegan–Carpenter numbers [99].

The flow of the low-speed motion of a body in superfluid ^{4}He must be potential. However, the movement of an oscillating body in a fluid is also associated with the movement of the volume and mass of the surrounding fluid. The additional mass of fluid will affect the kinematic drag coefficient, which is proportional to the amplitude of the body's oscillations (and the speed of its movement). The determination of the mass of an oscillating body will include an additional term related to the penetration depth of the viscous motion, which will be close to zero at low temperatures, where the density of the normal component ρ_n will be negligibly small.

The resonant frequency and the width of the frequency resonances of the oscillator in a liquid are affected by the forces of hydrodynamic resistance. In this case, both the reverse fluid flow around the oscillating body and the viscous resistance of the flowing fluid lead to a decrease in the resonant frequency and additional energy losses, which affects the quality factor of this resonant system. Thus, the effective mass of an oscillating body in liquid helium can be written as the sum of three terms:

$$m_{He} = m_{eff} + \beta \rho_{He} \mathcal{V} + B \rho_n A_s \delta .$$

Here, m_{eff} is the bare mass of the oscillator, the second term represents mass enhancement due to back flow, and the third term is the mass of the viscous layer attached to the oscillator. For a rectangular beam oscillating in the direction perpendicular its length L, $\mathcal{V} = TWL$, where T is its thickness, and W is its width ($L \gg T,\ W$), $A_s = 2LT + 2LW$ is the area of the side faces, ρ_{He} is the density of helium, and β and B are geometric constants of the order of unity. In superfluid helium at low

temperatures, the last term asymptotically approaches zero, so that only the term associated with the added mass affects the resonant properties of the oscillator.

In superfluid ^{4}He, the drag force of a mechanical oscillator at high velocities is approximately proportional to V, corresponding to a constant drag coefficient C_d, as is usually the case in turbulent motion in classical fluids. However, in contrast to classical liquids, the rate of transition from laminar to turbulent flow in superfluid helium occurs quite abruptly.

The methods used in the investigation of superfluid helium for the generation and detection of turbulence consist of tracking the motion of oscillating bodies under resonant conditions and measuring the speed of their motion, depending on the magnitude of the applied mechanical stresses. Vibrating grids, levitating spheres, superconducting wires, and quartz tuning forks are some of the resonators used extensively to study superfluids. Recently, micro- and nano-electromechanical systems (MEMS and NEMS) have begun to be used as small-size and vanishingly small mass resonators. At temperatures above 1 K, methods include rotating blades [43] and grids drawn along the channel [41, 42, 102–105], and the creation of fast flows with high Reynolds numbers around standing objects with the help of turbines [52, 106]. In Section 6, we shall focus on temperatures much less than 1 K, at which the normal component can be ignored and at which the methods of 'heat counterflow' and the 'washing machine with high Re' cannot be applied yet.

6. Oscillating resonant systems at low temperatures

Circular grid membranes [107–111]. The first experimental technique employed to study the generation of vortices at low temperatures was the excitation of resonant oscillations of a thin transparent metal grid custom made in the form of a circular membrane [107]. A nickel grid 90 mm in diameter (Fig. 9a) was sandwiched between two electrodes, each at distance of 1 mm from the grid, forming a dual capacitor. The mesh grid (75% transparency) had square cells with a thickness of 6 μm, width of 17 μm, distance between the metal strips of the grid of 111 μm, and grid mass $m = 85$ mg. The grid surface roughness was less than 2 μm. A high voltage (about 500 V, Fig. 9b) was applied to the grid, and an alternating voltage was applied to one of the electrodes (control), which made the mesh oscillate due to electrostatic attraction. The second electrode, owing to time-varying induced charge, served as a detector. The resonant frequency in different designs of the device was ≈ 1 kHz, while the quality factor of the oscillatory system in a superfluid liquid at low excitation voltages and low temperatures reached 2×10^5 [111]. A transition to the turbulent regime was observed at grid velocities of ≈ 2 cm s^{-1}. The maximum amplitude corresponding to such vibration was $A \sim 30$ μm.

Levitating sphere [112–115]. Another system to probe superfluid ^{4}He involved a ferromagnetic ($SmCo_5$) ball of diameter $D = 0.2$ mm with a bare mass of 27 μg levitated in the space between two superconducting plates of a flat

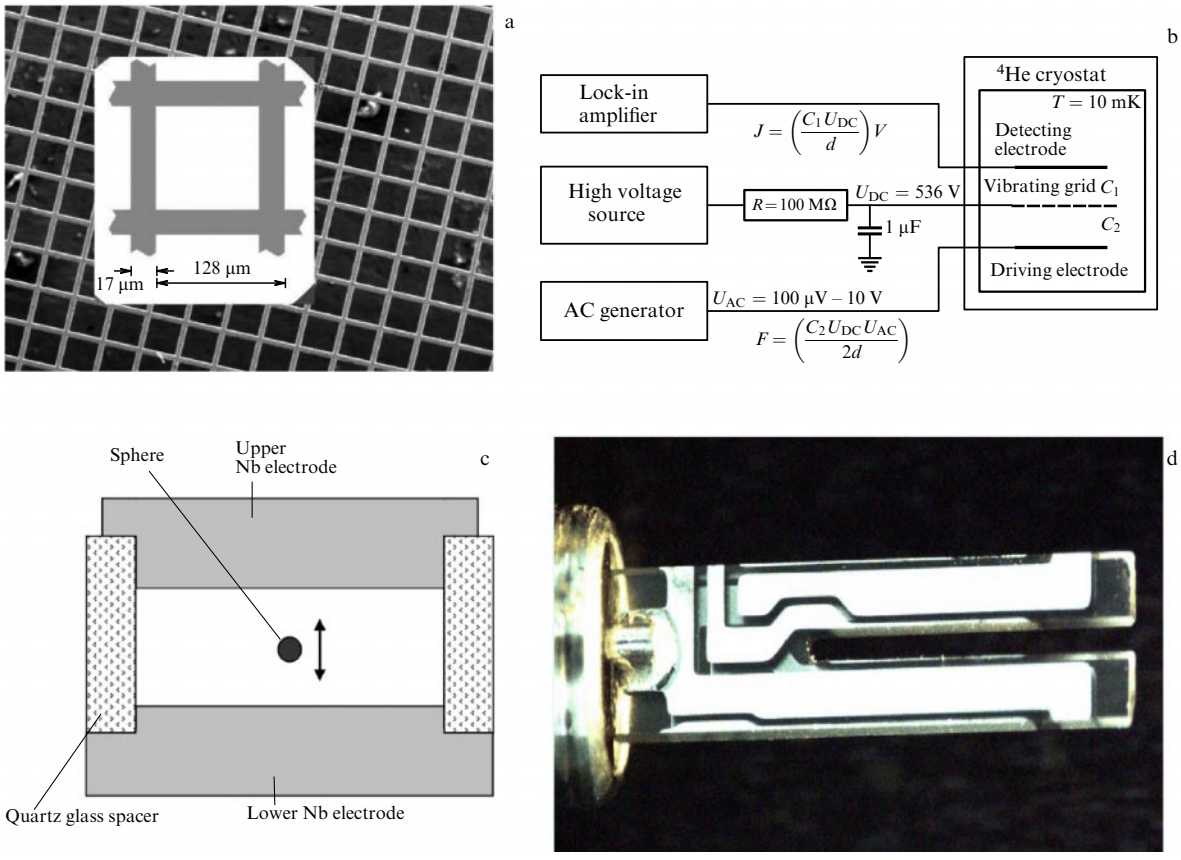

Figure 9. (a) SEM image of the nickel grid used in the study of quantum turbulence at low temperatures. (b) Schematic of these measurements [107, 109]. (c) Levitating magnetic sphere with a radius of 120 μm, distance between superconducting electrodes of 1 mm [112]. (d) Quartz tuning fork, prong length of 2–3 mm, resonant frequency, depending on the geometric dimensions and the excited mode, from 4 kHz up to 300 kHz (photo from open sources).

capacitor (4 mm in diameter) with a distance of 1 mm between the plates (Fig. 9c). The ball was charged up to ~ 1 pC during the cooling of the device until the superconducting transition of the niobium capacitor, at which point the sphere lifts in the space and levitates. Furthermore, an alternating electric field to one of the plates forces the sphere to oscillate at its characteristic resonant frequency ($f \approx 120$ Hz). The second plate picks up the induced charge, and the resulting current determines the displacement and speed of the sphere. The quality factor of the system at low temperatures in a vacuum reached 10^6, and about $\sim 10^4$ in superfluid helium at $T = 25$ μK. It was observed that the critical speed for transition to the turbulent regime was $V_{cr} \approx 1.94$ cm s^{-1}. The displacement amplitude corresponding to such a velocity was $A \sim 270$ μm. For a sphere with a radius of 75 μm (mass $m = 15$ μg), resonance $f = 236$ Hz, and $V_{cr} = 4.2$ cm s^{-1} was observed at all temperatures below $T = 1.6$ K [112]. In [115], the Q-factors of the sphere oscillations in the laminar regime were measured in a fairly wide temperature range. The results of these measurements are shown in Fig. 12 in Section 7.

Quartz tuning forks. Tuning fork (quartz) resonators have found wide application as a viscosity sensor for various liquids at different temperatures, including fuel level meters in car tanks. In recent years, quartz tuning forks have found wide application in low-temperature physics for the study of quantum turbulence. The advantages of such resonators include their mechanical rigidity, simplicity of installation, thermal cycle stability, high quality Q factor, and low cost. The most used quartz tuning forks have a resonant frequency of 32 kHz in air at room temperature. These resonators are used as a frequency standard in electronic watches ($f = 2^{15}$ Hz = 32,768 Hz) (Fig. 9d). A Q factor of 10^5 in a vacuum at low temperatures and 10^4 in superfluid helium in the absence of thermal excitations has been found. The dimensions of quartz tuning forks determine their resonant frequency. The tuning fork prongs have a width and thickness of the order of fractions of a mm, the length of the prongs varying from a few mm to tens of mm. The observed resonant frequencies of tuning forks used in low-temperature experiments were from 4 to 300 kHz. The critical velocities for the onset of quantum turbulence depends on the resonant frequency (Section 10). So, for the resonant frequency $f \approx 32$ kHz, $V_{cr} \sim 10$ cm s^{-1} and $A \approx 0.5$ μm. The effective mass of the tuning fork prong is $m \sim 400$ μg [116].

The technique for measuring the piezoelectric response of a quartz crystal (Fig. 9d) is shown in Fig. 10. One of the prongs is excited using an AC drive voltage, and the induced current (nA) in the second prong is measured using a lock-in amplifier with the help of a I–V convertor. A similar scheme was used to measure velocities of motion as a response to the exiting force for a grid oscillator (Fig. 9b) and levitating sphere (Fig. 9c).

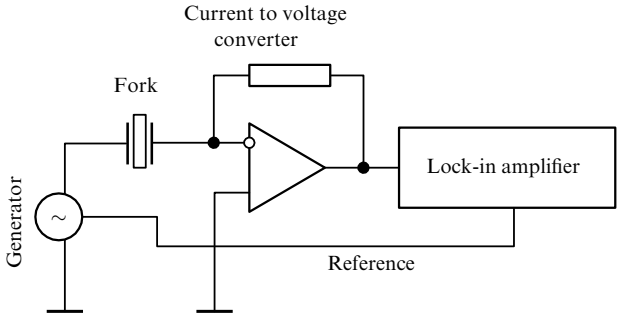

Figure 10. Scheme for measuring the inductive response of a piezoelectric system to an alternating electrical signal [116].

Superconducting wires in a magnetic field. This technique for the generation and detection of vortices has been used extensively in superfluid ^{3}He (see, for example, [117, 118]) (Fig. 11a). The essence of the technique is the measurement of the oscillation amplitude as the AC voltage of a superconducting NbTi wire with a diameter of 2–3 μm in a magnetic field of ≈ 25 mT under resonant conditions when an alternating electric current is passed through the wire. The induced EMF that arises on the wire when it moves in the magnetic field is proportional to the speed of the wire. The typical geometry of such resonators is shown in Fig. 11a; the distance between resonator legs ≈ 1 mm, wire curvature diameter ≈ 1 mm. The resonant vibration frequencies for such resonators are of the order of 1–3 kHz. The quality factor of such a system is $Q = 1000 - 3000$, $V_{cr} = 10$ cm s^{-1}, $A \approx 20$ μm, $m \approx 10$ ng.

MEMS and NEMS resonators. With the development of photolithography and micro-electronic technology, it has become possible to manufacture micro- and nanomechanical resonant systems, test them in superfluid helium, and use such devices as generators and detectors of quantum turbulence. Thus, in the last few years, investigations were done to study the interaction of MEMSs and NEMSs with vortices in superfluid helium at low temperatures.

Studies [120, 122–124] describe experiments with MEMS resonators consisting of a central plate $\approx 200 \times 200$ μm^2 suspended on curved springs at a height of 1.25 and 0.75 μm

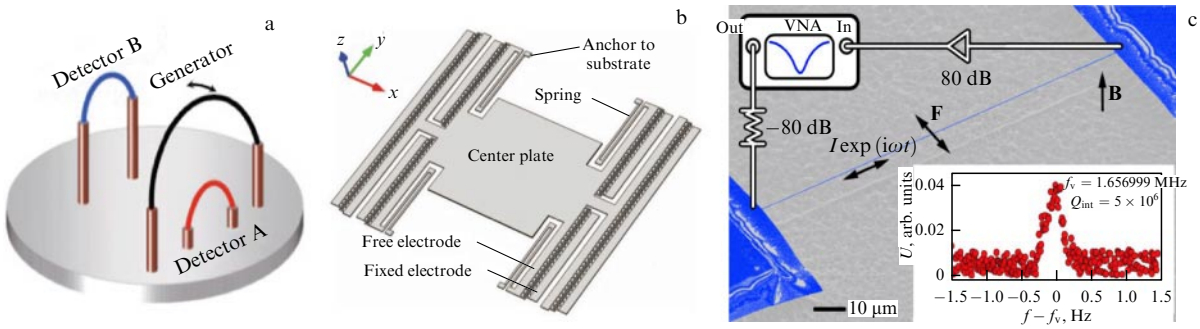

Figure 11. (a) Experimental device with oscillating superconducting wires with a diameter of 2.5 μm, using two of them as detectors and one as a generator of quantized vortices [119]. (b) EMS with the dimensions of the central moving plate ≈ 200 × 200 μm^2, distance from the substrate to the plate ≈ 2 μm [120]. (c) NEMS with the dimensions of an oscillating strip: thickness of 130 nm, width of 300 nm, length of 150 μm and its resonance curve, f_v is its resonance frequency, Q_{int} is the quality of the resonator [121].

from a substrate (for two tested systems). The masses of the central plates were 0.345 and 0.277 μg. The central plate was driven by electrostatic interaction between comb-drive actuators attached to its sides and stationary electrodes attached to the substrate (Fig. 11b). To improve the conductivity, a metal film was deposited on the structure. The manufacturing procedure for MEMSs is described on the manufacturer's website [125]. Depending on the distribution of constant charges on all electrodes, the resonating plate could oscillate with different modes, the amplitude of which was set by alternating electrical signals. The alternating current flowing in the system was proportional to the speed of the plate. The resonant frequencies for vibrations along the plane of the plate (direction x, Fig. 11b) were 24.1 kHz, perpendicular to the plane (in the direction z) $\sim$ 15 kHz. Two more rotational modes were observed with an axis along axis x $f \approx 25.6$ kHz and along the z-axis $f \approx 16$ kHz. The quality factor in vacuum reached 10^4. The surface roughness did not exceed 10 nm.

At the Quantum Technology Center, Lancaster University, UK, mechanical resonators with sizes of fractions of a micron have been developed and successfully used in the study of quantum turbulence [121, 126, 127]. The NEMS used in these experiments had the dimensions of resonant stripes $T = 130$ nm thick, $W = 300$ nm wide. The length of the strips was $L = 30$ μm and 150 μm and they were located at 1 μm from the substrate plate. The resonant frequencies for these two resonators were $f = 11.6$ MHz and 1.6 MHz. The main substrate material was undoped silicon; the resonator strip was made of silicon nitride (100 nm), on which an aluminum conductive layer of 30 nm was deposited during the manufacturing process. The mass of the resonant strip was $m \approx 15$ pg. Placed in a magnetic field of 10 mT, in a vacuum, the resonator had a quality factor of 5×10^6 at a temperature of 7 mK. Aluminum in such magnetic fields remained in a normal state. The schematic of the experiment and measuring equipment is shown in Fig. 11c. We will discuss the generation and detection of vortices by MEMS and NEMS systems in more detail in Section 14.

7. Quality factor of oscillating systems

To be used as a generator or a detector of quantum turbulence, resonators must have a very high Q factor. Therefore, it is no coincidence that, when indicating the Q-factor achieved by the aforementioned resonators, the measurement temperature is indicated. At high temperatures ($T > 1$ K), the quality factor of the resonator will be determined by the interaction with roton excitations in superfluid helium. At temperatures of 0.7–0.1 K, the quality factor is limited by interaction with ballistic phonons, and only at lower temperatures does the material of the resonator and the accuracy of its manufacture determine the energy losses of the device.

In Fig. 12 is shown the influence of the temperature of superfluid helium on energy losses of resonators of various designs under resonant conditions. For all the oscillating structures shown in the graph, the main losses are determined by thermal excitations in liquid helium, and only at temperatures below 0.3–0.1 K is the maximum sensitivity of such resonators achieved. The interaction of the oscillating resonator with phonons is proportional to T4 in a temperature range of 0.2–0.8 K; the dependence is plotted as dashed lines. For high-frequency NEMS resonators, one of the

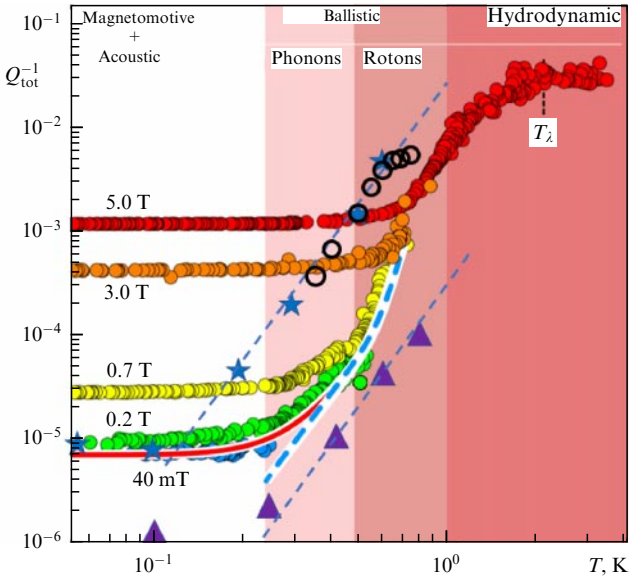

Figure 12. Graphs of temperature dependences of energy losses of various resonators in liquid ^{4}He. Dots of various colors are the results of loss measurements for an NEMS resonator in different magnetic fields (from [121]), resonant frequency $f = 1.6$ MHz; stars — grid loss data $P = 5$ bar, $f = 925$ Hz [111]; triangles — quartz tuning fork, $f = 6488$ Hz, $P \approx 0$ bar, recalculated from [129]; black circles — absorption measurement data for a levitating sphere $f = 237$ Hz [112].

significant reasons for the decrease in the quality factor of the system is magneto-mechanical losses, the magnitude of which is proportional to the magnitude of the magnetic field squared (left side of the graphic). Another effect that affects the quality factor of resonant systems at low temperatures is the dissipative losses of oscillating systems associated with the emission of sound waves.

8. Sound emission by oscillating systems

It is well known that vibrating bodies emit sound waves. For superfluid helium, in addition to the first sound, it is possible to emit waves of the second sound — the counterflow of the normal and superfluid components. For a plane oscillating in the direction normal to the plane, the amplitudes of two sound waves (first and second sounds) are determined by the relationship $\beta_e^2 T V_2^3 / C V_1$, where β_e is the thermal expansion coefficient, T is the temperature, V_1 and V_2 are the speeds of the first and second sounds, and C is the heat capacity. Thus, the energy transfer to the second sound radiation will be much weaker than to the first sound, except for special cases of resonant amplification of the second sound inside the experimental cell.

Quartz tuning forks, by analogy with musical tuning forks — standards of pitch — emit sound waves. The emission of sound waves will also occur at zero temperature, which can limit the quality factor of the oscillatory system at low temperatures. Theoretical models of sound radiation in an infinite medium were presented in [129, 130]. In the simplest case of acoustic emission, one can consider radiation into an infinitely large unbounded volume of a classical fluid with negligible attenuation of propagating sound waves. In this case, all the energy of the emitted waves is carried away from the source, and it is more or less easy to find an analytical expression for the radiation power of the oscillator, allowing certain simplifications regarding the geometry

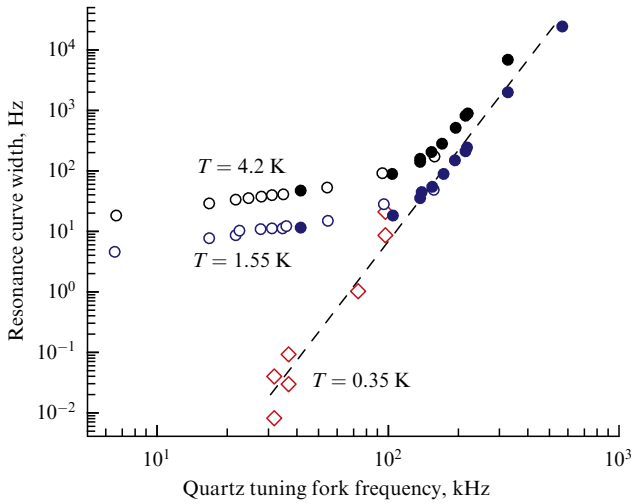

Figure 13. Dependence of the resonance curve width on the resonance frequency at different temperatures. Circles are the main modes of various quartz tuning forks, colored dots are the first overtones. Measurements at temperatures of 4.2 (black circles) and 1.55 K (blue circles), data from [129]. Red diamonds are the data from [130] at a temperature of 0.35 K. Results are given after subtracting the intrinsic losses of the resonators in a vacuum.

of the oscillator and ignoring the dissipation of sound waves propagating in the liquid. Models of emission of sound by vibrators consider three-dimensional (3D) and two-dimensional (2D) radiation. The calculations take into account two limiting cases: when the length of the sound waves is much larger than the dimensions of the emitter and when it is much less. The cutoff frequency for an oscillating system with dimensions of the order of several mm is $f_{gr} \sim 100$ kHz, and for dimensions of the order of several mm, $f_{gr} \sim 100$ MHz. For ordinary quartz resonators, as well as for micron superconducting filaments, the emitted waves can be considered in the long-wavelength limit.

Calculations of sound emission [131] showed that, for both 3D and 2D cases of wave propagation, the emitting power is determined, as for sound radiation by a long cylinder, by the relation

$$P = C_0 \omega^{n\omega} L_e^{nl} V^2 ,$$

where C_0 is a constant depending on the width and thickness of the oscillating body, on the speed of sound in the liquid, and on the density of the liquid; $n\omega = 5$ for 2D and cylindrical radiation, and $n\omega = 6$ for 3D; the exponent nl of the effective length of the oscillating system L_e is equal to 2 for 3D radiation and is equal to 1 for the other two cases; V is the speed of the emitter. It is possible to determine the energy loss of the resonator due to the emission of sound waves by comparing the quality factor of the system in a vacuum and in liquid under the same temperature. The influence of vibration frequencies of quartz tuning forks on the quality factor of resonators was determined experimentally in [129, 130] (Fig. 13). The dotted line on the graph corresponds to $\Delta f \sim f^5$. Fitting the experimental results showed that the three-dimensional acoustic emission model describes the experimental data better. At high temperatures and at low resonant frequencies, the hydrodynamic component of vibration energy absorption is dominant. For these temperatures, acoustic impedance becomes significant for frequencies above 100 kHz. At low temperatures (below 0.35 K), the acoustic component of oscillation damping can be significant already in the frequency range above 10 kHz.

Note that all the measurements presented here were carried out at very small oscillation amplitudes, so that the measured drag forces were proportional to the velocity. Thus, in [130], it is indicated that the main mechanism of energy dissipation at low speeds of the tuning fork prongs is associated with the emission of sound, and this mechanism was assumed to determine the mutual influence of the tuning forks on each other. At a much higher velocity of tuning fork vibration, quantized vortices are generated in superfluid helium, and the transfer of energy to the vortex system — so-called turbulent drag — begins to play a fundamentally important role.

9. Vortex generation by oscillations of solids

Measurements of the resistance to the movement of oscillating bodies showed that at low speeds the drag force is proportional to the velocity, which corresponds to the laminar flow of the liquid. When the critical value of the velocity is exceeded, the turbulent drag increases rapidly with a growth of the amplitude and the velocity of the oscillations. The change in the behavior of hydraulic resistance in liquid helium at high temperatures occurs rather gradually (as in ordinary liquids), but becomes sharp at low temperatures, although the transition to the turbulent regime occurs at approximately the same critical velocities. An example of such behavior is shown in Fig. 14.

As we noted earlier, the response of a resonant system and its transition to the regime of generation of turbulence are affected by the temperature of the liquid and the presence of excitations in superfluid helium, which actively attenuate the resonant oscillations of the device. In addition, the prehistory of the experiment has a significant effect on the transition to the turbulent state.

At low temperatures, the transition to turbulence is often accompanied by hysteresis: as the driving force increases, the transition to the turbulent state is accompanied by a sharp drop in velocity. As the excitation signal reduces, the velocity

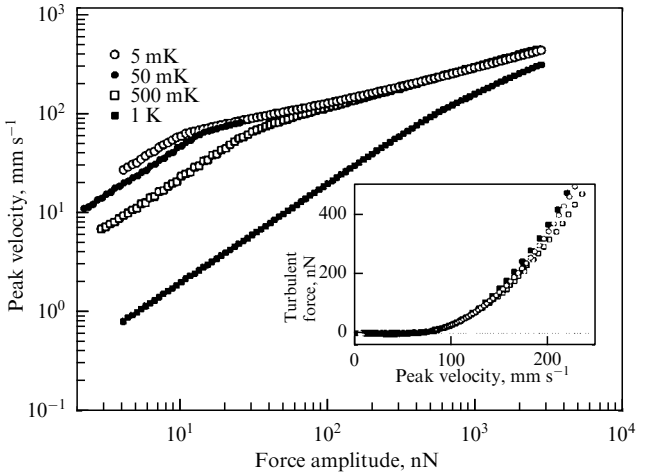

Figure. 14. Dependence of the maximum vibration velocity of a quartz tuning fork as a function of the driving force at different temperatures. Insert shows the additional driving force spended on generation of turbulence at different temperatures as a deviation from the linear laminar drag: $F_T = F - C_L V$. ^{4}He, $P = 1$ bar, $f = 32$ kHz, $V_{cr} \approx 8.5$ cm s^{-1}, results of [132].

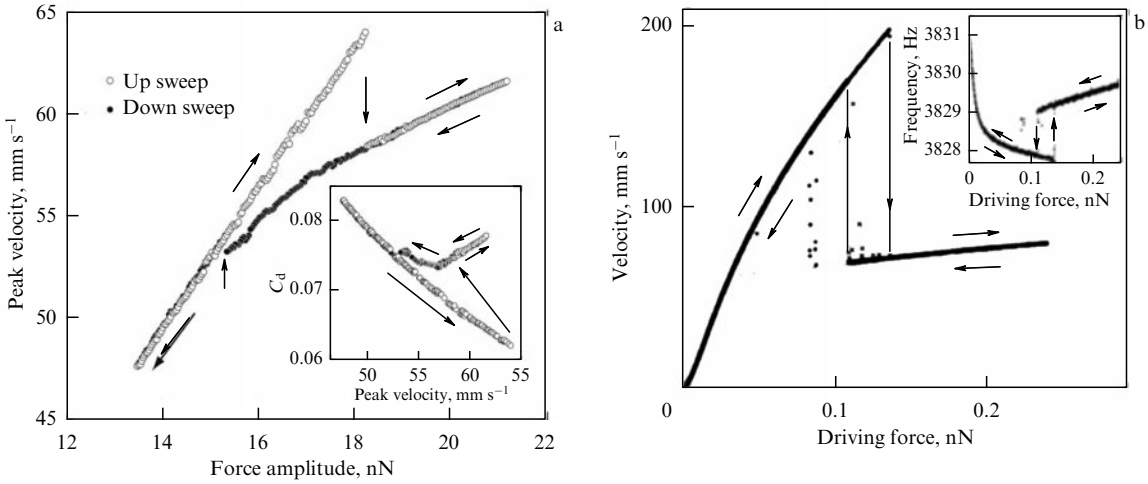

Figure 15. Hysteresis of transition to the vortex generation mode (a) for a quartz tuning fork: $T = 5$ mK, $f = 32$ kHz, $m \sim 400$ μg [132] and (b) NbTi superconducting wire ($d = 2.5$ μm, $T = 30$ mK, $f = 3.8$ kHz, $m \sim 10$ ng) [133] with excitation signal sweeping up and down in the system (driving force).

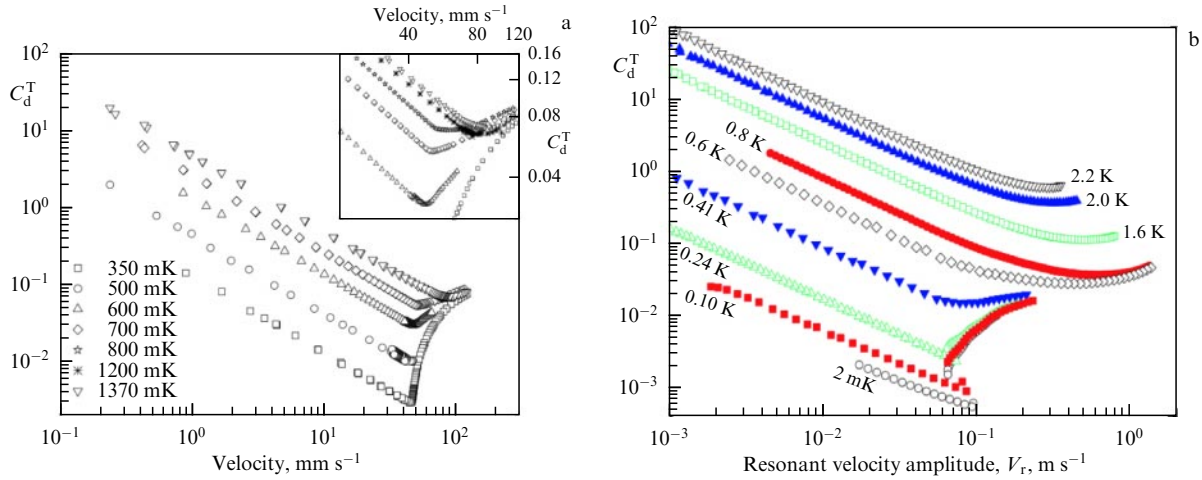

Figure 16. C_d^T drag coefficient as a function of the maximum oscillation velocity at different temperatures for (a) an oscillating grid [109] $f = 1080$ Hz and (b) for a quartz resonator $f = 6488$ Hz [127].

decreases to values measured at laminar motion, and there is usually a small jump in the increase of the motion velocity, corresponding to a state of potential fluid flow. The return to laminar motion occurs at significantly smaller forces and at lower velocities of the oscillator. Such behavior was observed for most of the oscillating systems used to generate vortices in superfluid helium (Fig. 15); however, the magnitude of the hysteresis and the conditions for returning to the laminar regime of oscillations strongly depend on many factors, including the mass of the oscillating body and the roughness of its surface. The hysteresis depends on the influence of individual vortices on the behavior of the oscillatory system, on the possibility of pinning vortices on the resonator surface, etc. The change in the behavior of the resonator during its transition from laminar to turbulent oscillations is clearly visible on the drag coefficient of the system (7). Moreover, if the laminar flow around an oscillating body is determined by the presence of excitations in superfluid helium (i.e., by temperature), then the transition to the turbulent state occurs at approximately the same speed of the vibration. Developed turbulence (reaching the stationary value of C_d^T) has a close value according to the dependence $F \sim C_d^T V^2$ in a wide temperature range, both in the presence of excitation in superfluid helium ($T > 1$ K) and at low temperatures (T down to mK). Along with the quadratic dependence of the resistance force on the velocity of the body, the transition of the flow regime from laminar to turbulent is accompanied by an increase in the value of C_d^T. For example, for the graphs shown in Fig. 16, C_d^T increases by 20–40 times at minimum temperatures. The change in the behavior of oscillations during the transition from laminar motion L of an oscillating body to developed turbulence TII can be explained by the existence of an intermediate region TI, in which individual vortices are generated by pinned vortices (see Fig. 19a in Section 12) due to an increase in the length of vortices when they move in a superfluid liquid together with an oscillating surface, self- and neighboring vortex reconnection, and ballistic motion of the resulting vortex loops (see Fig. 19b in Section 12). The presence of several critical velocities and different mechanisms of energy transfer from the resonator to superfluid helium was observed in experiments with free damping of grid oscillations at low temperatures. Experimental temperatures were 10 mK, pressure $P = 5$ bar, with high purity ^{4}He. At small initial amplitudes and velocities of grid oscillations $A_B < 3.5$ mm s^{-1} (experimental technique and geometry in Figs 9), the velocity corresponds to the movement of the middle of the grid, and the attenuation of oscillations is

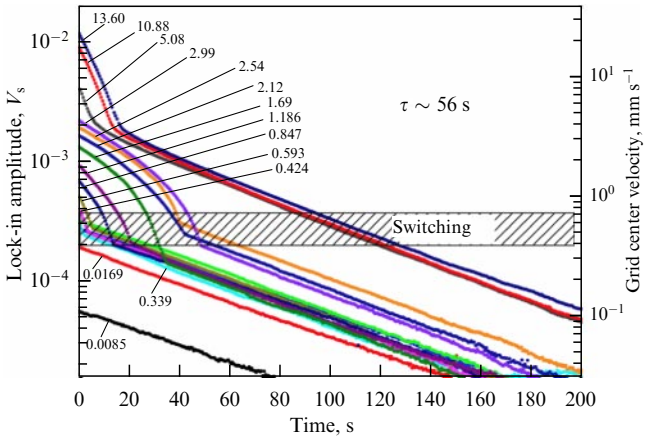

Figure 17. Free decay of grid oscillations at $T = 10$ mK, $P = 5$ bar, VDC= 500 V for different initial oscillation amplitudes. Top electrode signal (in V_s) is plotted as a function of time after stopping the harmonic driving voltage applied to the bottom electrode. Lowest drives give a decay time constant $\tau \sim 56$ s as laminar damping. The shaded region indicates where switching was observed in the response. The corresponding maximum grid velocities are plotted on the right-hand ordinate scale.

determined by the quality of the system and the laminar flow of the superfluid liquid. The free grid motion is described by the exponential damping with the exponent time $\tau \approx 56$ s. An increase in the initial speed of the grid leads to a change in the nature of the movement. It is seen in Fig. 17 that, for a speed of several mm s^{-1}, the energy losses of the grid increase intensively and this loss of speed continues to values of 0.4–0.7 mm s^{-1}, after which the mode changes to laminar damping of oscillations. If the initial grid velocity was greater than 10 mm s^{-1}, the termination of energy pumping into the system is accompanied by rapid damping followed by laminar damping. In accordance with the previous definitions, we also refer to these transitions as L, TI, and TII. At very large oscillation amplitudes (and grid movement velocities greater than 2–3 cm s^{-1}), a TIII turbulent state arose, characterized as a very rapid decrease in the oscillation amplitude with characteristic times of seconds, followed by laminar damping.

At low initial speeds of the grid movement, with an increase in the amplitude of oscillations in the TI mode, a switching mode appears at the amplitude of oscillations, when the maximum grid speed periodically changes (a discussion of this behavior is given in Section 13).

When generating turbulence by oscillatory systems, one can compare the effect of dimensions on the laminar–turbulent transition, for example, for spheres of different diameters. Experiments with a ball on an elastic suspension were presented in [134]. The ball radius was 3.5 mm, resonance frequency $f \approx 320$ Hz, $Q \approx 3000$, and critical velocity was $V_{cr} \approx 0.14$ cm c^{-1}. At similar vibration frequencies ($f \approx 236$ Hz) but at lower temperatures (with cooling to 25 mK) and a smaller sphere radius (75 mm), the authors of [112] determined the critical transition velocity as $V_{cr} \approx 4.2$ cm c^{-1}. A comparison of the Reynolds quantum numbers for these two cases showed the closed values of ≈ 50 and 30. These Re values were closed to Reynolds numbers obtained in [49] for a stagnant flow of the normal component (Fig. 2a). For two spheres with very different sizes at these temperatures (both 1.5 K and 0.3 K), $q^{-1} \gg 1$, i.e., exceeding the critical velocity VCr corresponds to the transition from the laminar flow to the V_{cr} turbulent state.

10. Influence of the frequency of oscillation on the critical velocity of the transition to a turbulent state

At low temperature experiments, it was found that the velocities of the resonator vibration at which the transition to the turbulent regime occurred depended significantly on the oscillation frequency. It was shown above that in superfluid ^{4}He the force of resistance to the movement of a mechanical oscillator at high velocities is approximately proportional to the square of the velocity, which corresponds to a constant drag coefficient C_d, as is usually the case with turbulent drag in classical liquids. The transition to turbulence in classical fluids is accompanied by a smooth change in the drag coefficient (see Fig. 8), while the transition to one-component superfluid turbulence occurs quite abruptly (see Fig. 16).

For a classical fluid at low speeds in a laminar flow, the dissipative drag force (Stokes drag) arises due to viscosity, and this force for an object oscillating with a high frequency is defined as $C_d^L = c_L\sqrt{\omega\nu}/V$ (see Section 4). This relationship is valid when the viscous penetration $\delta = \sqrt{2\nu/\omega}$ is small compared to the size of the object. This condition is certainly correct for standard quartz tuning forks in normal liquid helium. If the turbulent drag is equal to the Stokes drag, we may estimate the characteristic velocity of an object in a fluid at which turbulent vortex generation begins (8), $V_x \cong (c_L/c_T)\sqrt{\omega\nu}$. From this relation the speed of the onset of turbulence is proportional to the square root of the oscillation frequency times the viscosity of the fluid. The situation changes in superfluid helium, especially at low temperatures, when the superfluid at low velocities exhibits a purely potential flow without viscous drag. In this case, the quality of the resonant system is defined by its own losses, which can be measured in a vacuum. The onset of 'turbulent' resistance may not necessarily be strictly associated with the developed turbulence in the sense of the irregular motion of a vortex tangle. The increase in drag can be caused by the emission of single vortex rings, as shown in Section 9, in the TI mode.

From measurements of the decay of quantum turbulence [38, 61, 62, 135], there is more and more evidence that quantum turbulence behaves similarly to turbulence in a classical fluid with an effective kinematic viscosity, the value of which is usually written as a multiple of the circulation quantum of a superfluid fluid: $\kappa = h/m$, where m is the mass of an ^{4}He atom for superfluid ^{4}He, or the double mass of an ^{3}He atom for superfluid ^{3}He. The similarity between quantum and classical turbulence is supported by theoretical arguments [18, 136–138], experiments that investigate fluctuations in a superfluid flow [43, 139, 140], and computer simulations [141, 142].

By analogy with formula (8) for classical turbulence, one could expect the critical velocity of the onset of quantum turbulence in the form

$$V_{cr} \cong \sqrt{\beta_T \omega\kappa}\,, \tag{9}$$

where β_T is a constant of the order of unity, depending on the geometry of the flow.

The frequency dependence of the critical velocity given in formula (9) can be obtained using the dynamic scaling arguments for the vortex motion. These arguments were first used to explain the critical rate of turbulence formation by high-amplitude second sound waves [143, 144]. In [145],

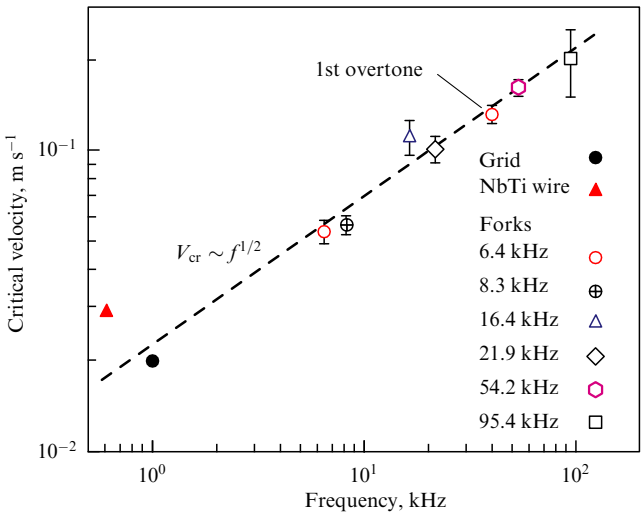

Figure 18. Influence of the oscillation frequency of resonant systems on the critical velocity of the transition to turbulence. Grid at $T = 10$ mK [111], superconducting wire at $T = 30$ mK [163], quartz tuning forks at $T = 5$ mK [128].

dependence (9) was rigorously obtained using dynamic scaling of the equations of vortex dynamics.

The first experimental confirmation of the frequency dependence of the critical velocity given by formula (9) was obtained in experiments with levitating balls [146, 147]. However, equation (9) should be valid only at relatively high frequencies, where the oscillation amplitude $A = V/\omega$ is small compared to the size of the object R. An experiment to test the influence of the oscillation frequency on the transition to turbulent generation of vortices was done with a set of quartz tuning forks [128]. In this work, the measurements were carried out on a comb of tuning forks, which were cut from a quartz plate with a thickness of $W = 75$ μm and a prong width of $t = 90$ μm. The distance between the prongs of the tuning fork was also the same, 90 μm. The length of the tuning fork prongs L determined their resonant frequency, which ranged from 6.5 to 300 kHz. The measurement results are shown in Fig. 18.

Critical velocities of the transition from the laminar to turbulent regime correspond to the relation $V_{cr} \approx \sqrt{0.7\kappa\omega}$, where κ is the circulation quantum. At lower frequencies, when the oscillation amplitude exceeds the size of the object R, it can be estimated that the critical velocity will become frequency independent [148]: $V_{cr} \approx \kappa/R$. The transition of the system to a turbulent state at amplitudes larger than the characteristic dimensions of resonating systems were observed in experiments with a grid and superconducting wires. The data from these experiments are also shown in Fig. 18. For the lowest resonant frequencies in experiments with a levitating ball, the critical velocities were significantly higher than those calculated by relation (9), which may be explained by the small number of pinned vortices, which is determined by the peculiarity of the experiments — the absence of contacts between the sphere and the chamber walls.

11. Dissipative processes in superfluid helium

At temperatures at which the normal and superfluid components exist, there is an interaction between the components, and, for homogeneous turbulence (Vinen turbulence), the energy transfer from the oscillating body to the vortex system is defined as

$$\epsilon = \nu'(\kappa^2 \mathcal{L}^2)\,, \tag{10}$$

where ν' is the effective viscosity, and the relation $\kappa^2\mathcal{L}^2$ is the effective root-mean-square vorticity of the superfluid component [149]. Thus, relation (10) can be an analogue of the energy flow in the inertial turbulence interval for classical Newtonian fluids. By analogy with classical fluids [5], energy is transferred to large eddies and flows through the Richard inertial cascade into the dissipation region, where the flow becomes laminar. The energy spectrum of such a process has the Kolmogorov form

$$E(k) = C_{\mathrm{K}} \epsilon^{2/3} k^{-5/3}\,,$$

where $E(k)\,\mathrm{d}k$ is the energy of the turbulent system per unit mass of the liquid, associated with the wave vector in the range from k to $k + \mathrm{d}k$, ϵ is the energy flux through the inertial cascade per unit mass, i.e., the pumping rate into the vortex system is equal to the rate of energy dissipation in the system (due to viscosity or with the help of another mechanism), and C_{K} is a constant of the order of unity. For a classical fluid, the energy dissipation is determined by the viscosity $\epsilon = \nu\langle\omega^2\rangle$, where $\langle\omega^2\rangle$ is the flow vorticity. In the range of wave vectors greater than l, energy transfer through the Richard cascade occurs due to vortex reconnections and the formation of smaller vortex loops, i.e., the process is semiclassical. In experiments with high Reynolds numbers (for example, the 'washing machine' [43]), it was experimentally shown that the semiclassical behavior of a vortex tangle only applies to length scales much larger than the average distance between vortex lines. However, any similarity between the classical and quantum velocity fields must disappear at length scales comparable to or smaller than the distance between the vortices. In this case, the flow of the superfluid component must be very different from the velocity field in the classical flow.

On scales of the order of or less than l, quantum effects (circulation quantization and, connected with it, the existence of vortex line cores) should strongly manifest themselves in the velocity field of the superfluid component. It can be assumed that, in the absence of viscosity of a normal fluid, the Kolmogorov spectrum and the corresponding energy flux from large scales to the region of small sizes, related to the motion of the fluid as a whole, will smoothly merge with the spectrum of quantum turbulence at $kl \to 1$. The velocity for the Kolmogorov spectrum can be rewritten as

$$V^2(k) = C_{\mathrm{K}} \epsilon^{2/3} k^{-2/3}\,. \tag{11}$$

Then, on a scale of lengths l, the characteristic velocity should be the same as for a homogeneous vortex tangle. This velocity is of the order of the velocity of the superfluid component at a distance l from a single vortex and is determined by the expression

$$V^2(l^{-1}) = \frac{\beta\kappa^2}{l^2}\,, \tag{12}$$

where the parameter β depends on the geometric arrangement of the vortices. With a smooth connection between equations (11) and (12) on the distances between the vortices ($kl \to 1$),

we obtain

$$\epsilon = \left(\frac{\beta}{C_{\mathrm{K}}}\right)^{3/2} \kappa^3 l^{-4} = \left(\frac{\beta}{C_{\mathrm{K}}}\right)^{3/2} \kappa^3 \mathcal{L}^2 = \nu'(\kappa^2 \mathcal{L}^2)\,.$$

With such a qualitative analysis, it turns out that the effective viscosity for quantum turbulence will be of the order of magnitude

$$\nu' = \left(\frac{\beta}{C_{\mathrm{K}}}\right)^{3/2} \kappa\,.$$

Thus, this quantity is of the order of the circulation quantum.

At low temperatures, the usual viscosity in liquid helium no longer exists, and a superfluid liquid requires another mechanism for the dissipation of the energy pumped into the system. One of the possible mechanisms may be reconnection processes, which lead to the appearance of Kelvin waves (waves moving along the vortex core). The distance between the vortices $l \approx \mathcal{L}^{-1/2}$, while the characteristic radius of the vortex loop for the case of uniform turbulence will be

$$\left\langle \frac{1}{R^2} \right\rangle \approx \frac{1}{l^2} = \mathcal{L}\,.$$

The speed of reconnections can be estimated from a dimensional analysis. During the interaction of a vortex tangle, there is one dimensional parameter — the average distance between vortices l — and the value l^2/κ can act as a time scale. Then, the rate of reconnections per unit volume of vortices should be of the order of $\kappa l^{-5} = \kappa \mathcal{L}^{5/2}$ [5].

Computer modeling has shown that, when a straight vortex and a vortex ring intersect and reconnect, Kelvin waves scatter on the newly formed vortices [150]. The reconnection of two straight vortices forms regions of high curvature on these new vortices, which, due to the tension of the vortex core, move at a high speed along the vortex. An experimental observation of reconnection processes was presented in the work of a group from Maryland, in which, by decorating vortices with hydrogen microparticles [151–153], it was possible to observe the formation of Kelvin waves [154, 155]. At high temperatures with a relatively high viscosity of the normal component, the curvature of the vortex rapidly decreases due to friction forces. At low temperatures, in the absence of viscosity, Kelvin waves with large curvature running along the vortex core emit phonons. The emission of phonons in a superfluid liquid at zero temperature can be the main dissipative mechanism of energy loss by a vortex.

For an isotropic vortex tangle with a distance between vortices l, the velocity field of the superfluid component acting on a neighboring vortex will be

$$V_{\mathrm{s}}(l) = \frac{\kappa}{2\pi l}\,.$$

The motion of the vortex line on the characteristic dimensions l is connected with the frequency as

$$\omega = \frac{\kappa}{l^2}\,.$$

This relationship is of fundamental importance for the emission of sound or phonons with frequency ω. If we consider two rectilinear vortices located at a distance of $2b$ and moving under the action of mutual velocity fields, then the rate of energy loss that they radiate during their mutual motion per unit length of the vortex will be [156, 157]

$$\frac{\mathrm{d}E_{\mathrm{L}}}{\mathrm{d}t} = \frac{\rho\kappa^7}{(4\pi)^5 c^4 b^6}\,,$$

where c is the speed of sound. Let us imagine that the vortex ring has a size of $2b$, which is equal to the distance between the vortices. The estimated time for the vortex ring to lose its size l and its energy will be defined as the rate of energy transfer of the vortex to Kelvin waves per unit mass of liquid. This value is of the order of magnitude [5]

$$\tilde{\epsilon} = G\kappa^3 l^{-4} = G\kappa^3 \mathcal{L}^2\,,$$

where the factor G is of the order of one. Thus, for the case of energy emission in the form of phonons due to kinks in the vortex lines, the effective dissipative parameter, the effective viscosity for the case of the absence of real viscosity in a superfluid liquid, is of the order of magnitude κ:

$$\nu'' = \zeta\kappa\,,$$

where the numerical factor ζ is in the range of 0.05–0.3 [26].

Spin-down experiments [38] on the decay of eddy turbulence at $T = 0.15$ K showed that the value of ν'' is close to 3×10^{-3}. However, it can be shown that there is a region of wave vectors $\approx l^{-1}$ for which turbulence is situated in the intermediate region between the Richard cascade and dissipation due to Kelvin waves. According to the theoretical concepts of [158], in the process of energy transfer to the high-frequency region, there is a bottleneck in the accumulation of vortex energy in the wave vectors of the beginning of the formation of Kelvin radiative processes, which can well explain such a small value of ν'' observed in experiments.

By analogy with the viscosity of classical liquids and the normal component of helium-II at high temperatures, one can estimate the ratio of the Keulegan–Carpenter number (KC) and the Stokes number β_{S} by introducing the concept of effective viscosity in accordance with the arguments given above and assuming for all experiments the parameter $\zeta = 0.11$. According to the results of these experiments (see Table), at temperatures at which we can ignore the concentration of the normal component, the transition to the turbulent regime for a variety of structures with different sizes is described by the relation $\mathrm{KC} \times \beta_{\mathrm{S}}^{1/2} \approx 14.9 \pm 5.1$.

For classical liquids, changing the Keleghan–Carpenter number and the Stokes number β_{S} transforms the structure of the generated vortices in the liquid. For water, it is possible to draw a rather conditional line of the difference in the behavior of the generated vortices. As noted above, at large KC values, the inertial forces in the fluid predominate during the movement of an oscillating structure, and at low Stokes numbers a turbulent mode of motion occurs. The transition from laminar to turbulent behavior takes place at a ratio of the oscillation frequency and viscosity in the system corresponding to equation (8). For a classical fluid, this transition is determined by the following relation:

$$V_x \cong \frac{c_{\mathrm{L}}}{c_{\mathrm{T}}} \sqrt{\omega\nu} A\,,$$

and the drag coefficient at the speed of transition to the turbulent regime is written as

$$C_{\mathrm{d}} = \frac{2\alpha_{\mathrm{s}} S}{A} \sqrt{\omega\nu}\, \frac{1}{V} = \frac{2\sqrt{2}\pi\alpha_{\mathrm{s}} S}{A} \frac{1}{\mathrm{KC}} (\pi\beta_{\mathrm{S}})^{-1/2}\,,$$

Table. Characteristics of experimental structures and Keulegan–Carpenter number (KC) and Stokes number (S) calculated for them.

Structure	d, μm	f, kHz	V_{cr}, cm s^{-1}	KC_{cr}	β_S
Schoepe sphere [114]	248	0.12	1.9	0.64	671
Schoepe sphere [112]	200	0.24	3.8	0.79	873
Osaka wire [133]	2.5	0.7	5.0	28.6	0.40
Lancaster wire [160]	4.5	1.0	4.8	10.7	1.84
Lancaster grid [108]	21	1.0	4.5	2.14	40.1
Osaka wire [119]	2.5	3.8	7.0	7.37	2.16
Tuning fork [128]	75	6.5	6.5	0.13	3.3×10^3
Tuning fork [161], $T > 1$ K	400	32	6.0	4.7×10^{-3}	4.6×10^5

where S is the area of the moving body, A is the cross section of the body, and the coefficient for the cylinder is $\alpha_s = (3\pi/4)\sqrt{2}$. Thus, the transition to turbulent flow at values $C_d \approx 0.5-2$ will occur at the ratio $KC \times \beta_S^{1/2} \approx 10$. In work on the visualization of the formation of vortices during the oscillation of a cylinder [99], the transition from a two-dimensional vortex structure of the Karman vortex street to a three-dimensional one (i.e., the regime of developed turbulence) occurred at $KC \times \beta_S^{1/2} > 30$. Measurements of vibrations in superfluid helium of three quartz tuning forks at temperatures above 1.4 K [97], where the viscosity of the normal component cannot yet be disregarded, showed that the transition occurred at $KC \times \beta_S^{1/2} \approx 17$.

Thus, the characteristic ratios $KC \times \beta_S^{1/2}$ for the transition of a fluid around an oscillating body to a developed turbulence regime for both a classical fluid and superfluid helium at high and low temperatures have close values.

12. Influence of pinned vortices on the generation of quantum turbulence

As experimental studies show, the critical velocities of the transition to turbulent vortex formation fundamentally change after the first creation of vortices in the liquid volume — with the second and subsequent increases in velocity, the critical velocities usually become significantly lower. The generation of vortices by the counterflow of the normal and superfluid components requires the presence of vortices in the bulk of the liquid; otherwise, the growth of turbulence (and the temperature gradient) occurs only as the vortex front diffuses from the heater or from the cold end of the pipe [90]. For the creation of vortices from the wall of the vessel, speeds of the order of 10 m s^{-1} are required; just such velocities of ion movement create the quantized vortex rings. Similar arguments are valid for the generation of vortices during the oscillation of resonant systems at low temperatures, with the only difference being that the movement proceeds via an oscillating body relative to a stationary fluid. Thus, to increase the number of vortices in the volume, it is necessary to have some remanent number of vortices connected with the vibrating body. A diagram depicting the pinning of vortices on oscillating structures is shown in Fig. 19a. Figure 19b shows the formation of a vortex loop during the reconnection of the vortex to itself during the vibration of the oscillator.

The most revealing experiments in this regard were those on the use of oscillating wire resonators, in which the speed of the transition to a developed turbulence was determined by

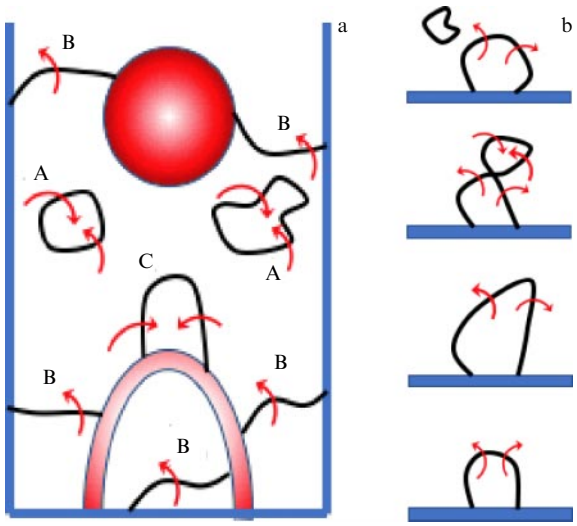

Figure 19. (a) Different positions of remanent vortices in a cell: A — residual vortices in the volume (remanent vortices), B — pinned vortices on parts of the device, for example, on a ball or wire (pinning vortices), C — intermediate case, when the vortex has weak fixation, it can crawl into position (B) or break away and become free (A); (b) growth of the length of the pinned vortex as the substrate moves away from us, followed by the formation of a free vortex loop (from bottom to top). Arrows show the directions of flow of the superfluid component around the vortices.

the ability of the oscillator to pin vortices. In experiments of the H Yano group on generating turbulence using an NbTi superconducting wire with a diameter of 2–3 μm, it was shown that the transition from laminar to turbulent motion occurred at wire speeds above 35 cm s^{-1}. With especially careful filling of the cell with superfluid helium (at a temperature below 100 mK in 20 h), it was apparently possible to fill the volume under study with a minimum number of remanent and pinned vortices. In this case, the first increase in the excitation signal under resonant conditions of such an oscillatory system led to the fact that the wire speed could reach values up to 1 m s^{-1} without transition to a turbulent state [162, 163] (virgin state). After the formation of a turbulent state, the return to laminar flow with a decrease in excitation occurred at significantly lower velocities. An example of such a hysteresis is shown in Fig. 15b. The next transition to the turbulent state after the laminar one occurs at lower vibration velocities (regular state).

Moreover, two identical resonators made of identical wires and placed side by side on a substrate exhibited different resonant properties. One of the wires at sufficiently low velocities began to generate vortices, while the other one

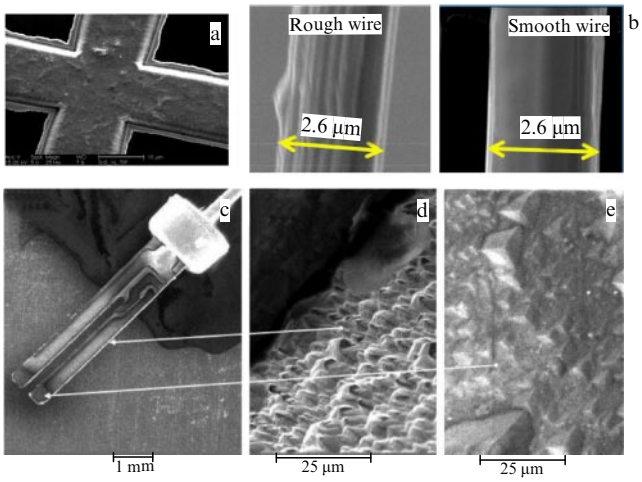

Figure 20. Micrographs of the surfaces of various oscillators: (a) metal mesh (from [164]); (b) NbTi superconducting wires, on the left with a rough surface and on the right with a smooth one (from a private communication by Professor Hideo Yano, Osaka City University, Japan). Surfaces: (c) of a quartz tuning fork, (d) of a quartz tuning fork with gold evaporation, and (e) of a monocrystal (from [165]).

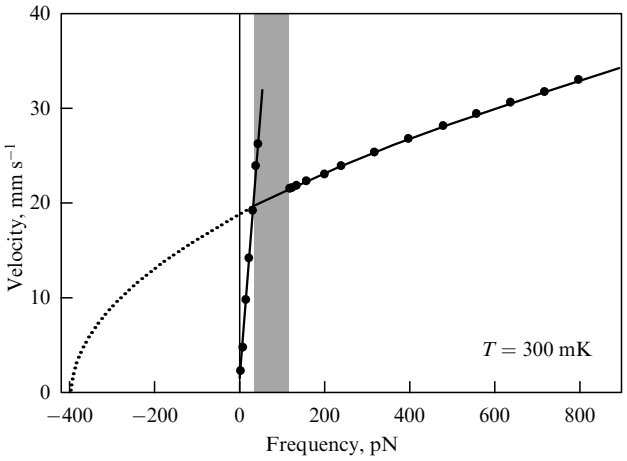

Figure 21. Dependence of the speed of a sphere on the magnitude of the applied force. Sphere size of 200 μm, oscillation frequency of 114 Hz, $T = 300$ mK, $V_{cr} = 2$ cm s^{-1}; in the gray region is an unstable transition to the turbulent state [166].

experienced laminar flows at significantly higher velocities. It should be noted that this behavior was observed only for superconducting wires: a significant excess of the velocities of motion over the regular transition to the state of developed turbulence. This feature can be explained by the different abilities of vortex pinning by the surface roughnesses of different structures. Figure 20 shows micrographs of various surfaces of oscillating systems.

A smooth wire (Fig. 20b, on the right) demonstrated a transition to the turbulent state at velocities several times higher upon increasing external excitation than the inverse transition to the laminar state upon decreasing the motion velocity ($V_{cr}^{T}/V_{cr}^{L} \approx 20$). Roughness with dimensions on the order of several micrometers for other systems (oscillating grids, a levitating ball, quartz tuning forks) led to the observed hysteresis being much smaller for them. In addition to a significant hysteresis at the 'onset and 'discontinuation' of turbulence, the pinning of vortices leads to an interesting effect — an unstable transition to turbulence.

13. Unstable transition to quantum turbulence

Experiments have shown that, in the operation of any generators of turbulence by oscillating bodies in superfluid helium, three regimes can be distinguished: low speed — laminar motion — when the force of hydrodynamic resistance F_d to body motion is proportional to the velocity $F_d \sim V$; high velocity, when the force is proportional to the velocity in the square $F_d \sim V^2$, along with these two main modes of motion of bodies in a superfluid liquid, there is an intermediate region of transition from laminar to turbulent motion, in which the creation of vortices and the transfer of energy from the mechanical motion of the body into the motion of the liquid have a probabilistic character. Figure 21 shows the results of measuring the speed of a levitating ball as a function of the applied variable forces [166].

Such a probabilistic transition to turbulence, as well as switching the detector to the detection mode, which will be discussed in Section 14, is described by the cumulative distribution function $F(t)$, which is the probability that a random variable has a value of no more than t, for example, a device failure occurs before the time t. Figure 22d shows a survival function (reliability function) $R(t)$, which describes the probability of an object 'surviving': $R(t) = P(T > t)$, where t is the time during which the events were observed, T is a random variable denoting the moment of 'death', and P means the probability of 'death' (failures) in a given time interval (the oscillator falls into the generation of vortex turbulence).

Statistical processing of the experimental results of the transition of a vibrational sphere into a turbulent regime showed that the temporal dependence is

$$R(t) \sim \exp\left(-\frac{t}{\tau}\right),$$

and it corresponds to the Rayleigh distribution, where τ is the mean lifetime. The average 'lifetime' (the time for the system to cross over to a turbulent state) does not depend on the temperature at $T < 0.5$ K, at which we have a sufficiently small number of thermal excitations in superfluid helium. Obviously, the average lifetime $\langle\tau\rangle$ depends only on the turbulent drag force $F_T = F - \lambda V_T$, defined as the difference between the applied force and the linear laminar dependence. The average lifetime of the system before the transition to turbulence can be described by the exponential

$$\langle\tau\rangle = \tau_0 \exp\left(\frac{F_T}{F_l}\right)^2,$$

where $\tau_0 = 0.5$ s and $F_l = 18.3$ pN.

Similar observations were made in the study of grid oscillations at low temperatures (Fig. 17, shaded area), where the switching mode occurs with a change in the grid oscillation speed (Fig. 23).

Thus, we can conclude that, during the transition from laminar motion of oscillating bodies to turbulent at low temperatures, processes of random switching of the flow around a moving body quite often occur: vortices begin to be generated, which leads to energy loss by the moving body and a decrease in the speed of its movement — which means a return to laminar motion. This switching regime falls on the TI region, where separate eddies are generated, in contrast to

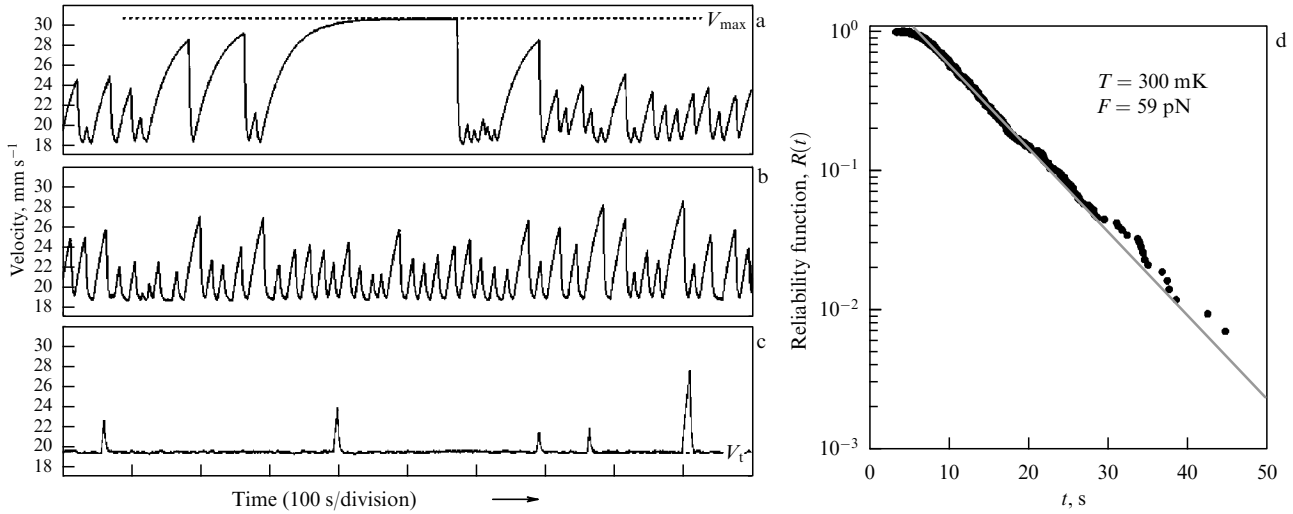

Figure 22. Dependence of the speed of a sphere on time with driving forces on the electrodes of the capacitor (a) $F = 47$ pN, (b) $F = 55$ pN, (c) $F = 75$ pN; V_t is the speed of transition to a turbulent state. (d) Survival function (reliability function) describing the probability that the sphere remains in laminar motion; temperature of 300 mK [166].

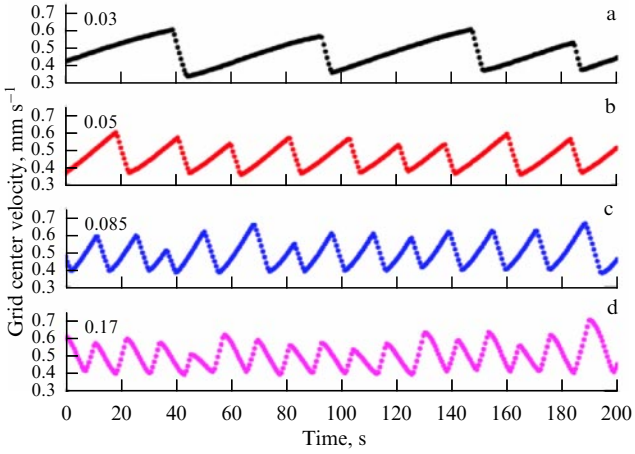

Figure 23. Switching of grid oscillation speed in the TI mode. Grid vibration is excited by an alternating voltage U applied to the driving electrode (in Fig. 9b): (a) $U = 0.03$ mV; (b) $U = 0.05$ mV; (c) $U = 0.085$ mV; and (d) $U = 0.17$ mV.

the TII regime — developed turbulence. The features of vortex emission in the TI and TII regimes will be considered in more detail in the next section.

14. Detection of quantum turbulence

One of the main questions that arise in the study of quantum turbulence is understanding how far and how fast the region of a turbulent state in superfluid helium can propagate after the start of vortex generation. If, say, in quasi-one-dimensional geometry, vortices are created at the origin of coordinates due to some mechanism described above, and in the process of diffusion or ballistic flight vortices lose energy and momentum, then vortex turbulence propagates only to a finite distance, and only part of the space in this case will be occupied by vortices. In the general case, this resembles the situation with the calming of a river after the rapids. Let us consider experiments in which vortices were detected at some distance from the turbulence source and estimate the vortex generation rate.

As we noted earlier, the formation of quantum turbulence is possible in two different ways — thermal and mechanical. With the thermal method, the generation of vortices occurs due to the counterflow of the normal and superfluid components during local heating of helium. In this case, it is assumed that the establishment of a counterflow in the entire volume of the heat flux occurs in times determined by the speed of propagation of the second sound, i.e., 15–20 m s^{-1} at temperatures from 1 to 2 K. For a sample size of several cm, this time is of the order of milliseconds. At lower temperatures, the concentration of the normal component becomes negligible, and the counterflow of the two components can be disregarded.

The creation of vortices by the mechanical method occurs when bodies move in superfluid helium with velocities above the critical ones (Section 9 and 10). Now, we are interested in the processes of registering the movement of vortices in space at different temperatures.

The possibility of decay of vortex turbulence due to the motion of vortex loops and their disappearance on the walls of the vessel was expressed in the first studies of quantum turbulence [168]. Created in a superfluid helium and moving in it, quantized vortices will behave differently depending on the temperature of the liquid. At ultralow temperatures, when thermal excitations in the Bose fluid can be ignored, vortex rings will propagate without changing their dimensions. The speed of motion of a vortex ring of radius R_0 at zero temperature is given by the expression [8]

$$v_0 = \frac{\kappa}{4\pi R_0}\left(\ln\frac{8R_0}{a_0} - \frac{1}{2}\right).$$

It is not difficult to see that the speed of the ring becomes smaller as its radius increases. For a vortex ring with a radius of 1 μm, the vortex velocity is of the order of $v_0 = 8$ cm s^{-1}, for a radius of 10 μm, $v_0 = 1$ cm s^{-1}, and for a radius of 100 μm, $v_0 = 1.2$ mm s^{-1}. The characteristic times of passage of the distance to the detector via the vortices, say, for $D = 1$ mm, will be 12.5 ms, 100 ms, and ≈ 1 s, respectively. Of course, these values are only estimates. Diffusion or ballistic span times will be significantly affected by the complex shape of vortex rings with a large number of local

bends, reconnection processes, especially at the initial stages of vortex motion, and their high concentration with the decay of large vortices into smaller ones, as well as the processes of merging of small vortices with the formation of larger vortex loops.

A theoretical consideration and computer simulation of the processes of motion of vortex rings at zero temperature was carried out in [169, 170]. It was assumed in the calculations that the circular vortex rings began to diffuse in the mutual vortex fields of the superfluid component. In the process of movement, the vortex loops deformed and intersected with other ones and with themselves with the formation of small loops from large ones and the merging of small loops into large ones. The calculations were made within the local approximation of the Biot–Savart equation [171]. Computer simulation has shown that, for times of the order of 1–2 ms, a fairly wide distribution of vortex loop sizes (up to tens of μm) forms vortex rings with a diameter of the order of 1 μm. The decay times of turbulence in a volume with dimensions of 160 μm were of the order of several ms. During this time, most of the vortices leave this region. This made it possible to estimate the average velocities of vortex motion at 4 cm s^{-1}. Similar results were obtained in computer simulations of the generation of vortices by a levitating sphere [172]. Computer simulation within the framework of the Biot–Savart equation [173] indicated a slowdown in the speed of motion of vortex loops with a large number of kinks and associated Kelvin waves. However, the order of velocities and times of motion of the vortices must be preserved. The results of computational experiments on the ballistic expansion of small vortices from the region of turbulence generation are in good agreement with the results of theoretical work [174] on the diffusion decay of vortex turbulence.

Experimental observations of the detector response to the generation of a turbulent state by a moving body located at a macroscopic distance from the detector were made using high-Q resonators. Thin superconducting wires, quartz tuning forks, and micro- and nanoelectromechanical systems (MEMS and NEMS) were used as such detectors.

The change in the oscillation frequency of a high-quality resonator when a vortex is attached to it will increase due to an increase in the returning force associated with an increase in the length of the vortex when the resonator moves, i.e., the oscillation frequency of the resonator will increase. On the other hand, we note that any pinning of the vortex to the resonator is an incorporation of additional mass, which should reduce the frequency of the resonator. By the way, a similar effect of reducing the frequency of the resonator is observed in a superfluid liquid compared to a vacuum during laminar motion of the oscillating element of the resonator due to the added mass.

The question of the inertial mass of a vortex pinned on a detector is not completely clear at present. When considering the analogy between superfluidity and electrodynamics [175], the vortex energy E_v can be compared with its mass M_v through the Einstein relation $E_v \approx M_v c^2$, where c is the speed of sound. The complexity of the assessment is also related to the fact that the value of the added mass of the vortex will be affected by the pinning potential and the degree of slip of the vortex relative to the oscillating body, the density of pinned vortices, the Magnus forces acting on the vortex when it moves with the resonator element, etc. [176, 177]. So, the change in the frequency of the resonator with vortices has not been fully elucidated, and only experiments can answer this question by changing the frequency of the resonator under specific conditions.

In the work of Japanese researchers [178–180], who were the first to record the response of a detector located at a macroscopic distance from the generator to the formation of a turbulent state at temperatures of $T = 30$ mK, they observed that the detector frequency increased after the arrival of vortices. Both the generator and the detector were resonators in the form of an arc ≈ 1 mm in diameter made of NbTi superconducting wires with a diameter of about 2.5 μm (Fig. 11a). Excited by an alternating electric current in a magnetic field, the wire moved at maximum velocities of 50 cm s^{-1} and at characteristic resonant frequencies of $f \sim 3$ kHz and had an oscillation amplitude of the order of 27 μm. The mass of such a resonator was $m \sim 10^{-8}$ g. The distance between the detector and the generator, which differed in resonant frequencies by several hundred Hz, was ~ 1 mm in the experiments. A resonator with velocities up to 50 cm s^{-1} was used as a detector. Such high velocities correspond to the supercritical mode of operation of the detecting wire, exceeding the transition to the turbulent state (for a wire with a rough surface, $V_{cr} \sim 5$ cm s^{-1}). A significant excess of the speed of motion of the detecting wire is possible due to the fact that, as the authors of [162, 181] indicate, there were no residual pinned vortices on the detector. An increase in the velocity of the detector was accompanied by an expected decrease in the frequency of the laminar motion of the wire. The arrival of vortices at the detector after turning on the turbulence generator (a similar wire resonator with a movement speed of more than 10 cm s^{-1}) triggered the transition of the detector to the generation of vortices, which led to a sharp decrease in the detector oscillation amplitude and an increase in its resonant frequency by 0.3 Hz. After reducing the current through the detector (driving force) to a critical value ($F \approx 100$ pN) and turning off the vortex generator, the detector returned to laminar oscillations after some time.

At significantly greater distances (10 mm), registration of eddy turbulence was observed in studies of the Lancaster group [182]. Quartz tuning forks were used as a generator and a detector in these experiments. The vibration plane of the quartz tuning forks was parallel to each other. The resonant frequency of the quartz resonators used in these experiments was ~ 32 kHz, but differed for the generator and detector, which precluded the mechanical influence of one resonator on the other.

Experiments have shown (Fig. 24) that, at the freezing temperature of roton and phonon excitations, the formation of a turbulent state by one of the quartz tuning forks ('turbulence generator') affects the quality factor of the second tuning fork ('detector'), the speed of oscillation of the prongs of which was significantly lower than V_{cr} (0.3 mm s^{-1}). The 'detector' frequency also increased upon interacting with the vortices. In the 'telegraph' regime of switching on a 'generator' (2 s on and a rest period of 20 s), the amplitude of the 'detector' signal changed over times of the order of fractions of a second. Thus, at times of the order of fractions of a second, the vortices traveled distances of the order of ten mm to the second tuning fork ('turbulence detector'), reducing its quality factor. For times of a fraction of a second after the 'generator' was turned off, the quality factor of the 'detector' returned to its original value. According to the response of the 'detector', two critical rates of formation of vortices by the 'generator' can be distin-

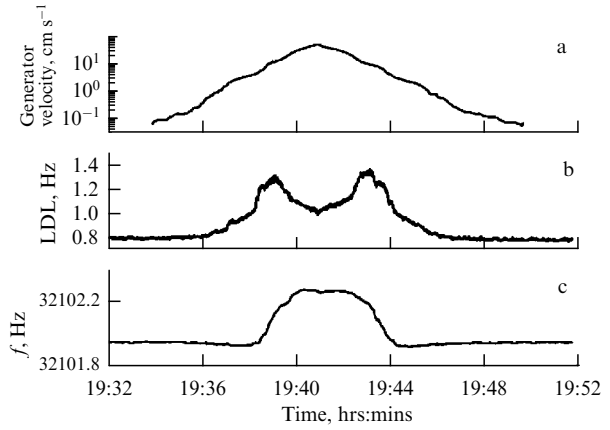

Figure 24. Influence of the 'generator' oscillation speed upon the amplitude of the external pump signal sweeping up and down (a) on the width of the 'detector' resonance (low-drive-linewidths — LDLs) (b) and its resonant frequency (c) $V_D \sim 0.3$ mm s^{-1}, $T = 10$ mK, $P = 5$ bar, extra pure ^{4}He [182].

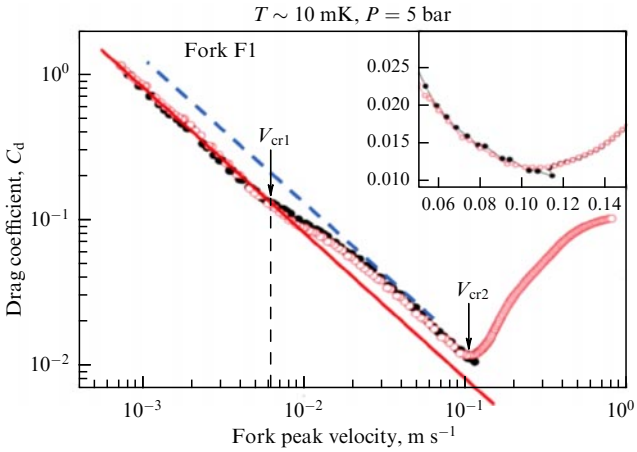

Figure 25. Drag coefficient C_d as a function of the speed of a quartz tuning fork. The black dots show the behavior of C_d if the external pump is reduced until V_{cr2} is reached.

guished. When the first critical speed ($V_{cr1} \sim 1$ cm s^{-1}) is exceeded, vortices begin to form, the number of which and their influence on the quality factor of the 'detector' increase with the speed of movement of the prongs of the 'generator'. When the turbulent state of the 'generator' is reached (the speed of movement of the prongs of the 'generator' exceeds $V_{cr2} \sim 15$ cm s^{-1}), the quality factor of the 'detector' begins to increase, which may indicate a decrease in the number of vortices that reach the detector, i.e., there is a 'shielding' by a vortex tangle that occurs near the 'generator' of the passage of vortices to the 'detector'. When the 'detector' oscillation speed exceeds V_{cr2}, the 'detector' ceases to change its quality factor and respond to the creation of vortices by the 'generator'. Decreasing the oscillation amplitudes of the 'generator' to the detection regime and increasing the amplitude of the 'detector' to generation gives a similar picture of the recorded signals.

A decrease in the response of the detecting wire at high generator powers and a more intense production of vortices was noted in the work of the Yano group [183]. As in experiments with quartz tuning forks, the decrease in the response of the wire detector with an increase in the intensity of vortex generation by the generator can be explained by the screening of the vortex flow by the turbulent state of the vortex tangle near the generator.

The detection of the propagation of vortices generated by a quartz tuning fork located at a distance of 5 mm from the MEMS is described in [124]. The MEMS, consisting of a 125×125-μm^2 central oscillating plate suspended at 2 μm above the substrate, was immersed in ^{4}He along with a quartz tuning fork as a turbulence generator. The vibration plane of the prongs of a quartz tuning fork was parallel to the plane of the resonator plate. The resonant frequency of the MEMS was 23 kHz. The measurements were carried out at a temperature of 15 mK. It turned out that, when the quartz tuning fork exceeded velocity $V_{cr} \sim 71$ mm s^{-1} at which turbulence generation begins, the damping of the MEMS resonator increased, but this increase depended on the intrinsic mode of the MEMS resonator and the ability to generate vortices by the resonator itself.

Note that the authors [124] of the work investigated the MEMS resonator itself for the possibility of generating vortices. Increasing the plate speed to 5 mm s^{-1} changed the hydraulic resistance coefficient — it stopped growing and became constant. At a speed above 140 mm s^{-1}, the drag coefficient of the oscillating plate of the MEMS resonator dropped sharply. The authors of [124] attribute this behavior to a change in the vortex pinning regime: at a high speed of motion, the resonator plate is cleared of pinned vortices.

The same features of the transition to developed turbulence are observed in the dependences of the drag coefficient of quartz tuning forks on their velocity. Peculiarities in the dependences $V(F)$ of quartz tuning forks at V_{cr1} were observed in many experiments at low temperatures (Fig. 25). The behavior of $C_d(V)$ is reproducible if the maximum speed of movement of the prongs of the quartz tuning fork is less than V_{cr2}. However, if the resonator switches to the developed turbulence mode $V > V_{cr2}$, then the experimental dependences in the low-velocity region become closer to the values denoted by the dashed line, and this behavior will also be reproducible after the transition to turbulence.

Comparing the results of the transition to turbulence (Section 12) and the data given above, we can assume the following scenario for the development of quantum turbulence. For the first generation of vortices (virgin state), the mode of transition to turbulence is determined by a small number of remanent vortices pinned on the oscillator. The number of pinned residual vortices on the oscillator can change with time (Fig. 3). As the speed of the oscillator increases above V_{cr1}, the vortices pinned on the oscillator begin to increase their length and intersect with themselves or with their neighbors as they lengthen, forming free vortex loops that can freely move in the liquid (as shown in Fig. 19b). V_{cr1} is on the order of 1 cm s^{-1} for many experiments at low temperatures. The number of generated vortices depends on $V - V_{cr1}$. At V_{cr2}, there is a transition to the generation of a large number of vortices, which do not have time to leave the vicinity of the oscillator and create a dense tangle of vortices, which can already serve as an obstacle to the flow of vortices into the surrounding space. The same tangle can interact with vortices pinned on the oscillator; vortices from the tangle can attach to the oscillator, increasing the density of pinned vortices.

The difference in the value of V_{cr1}, and sometimes the complete absence of the transition to the TI vortex production regime, is due to the absence or negligible number of

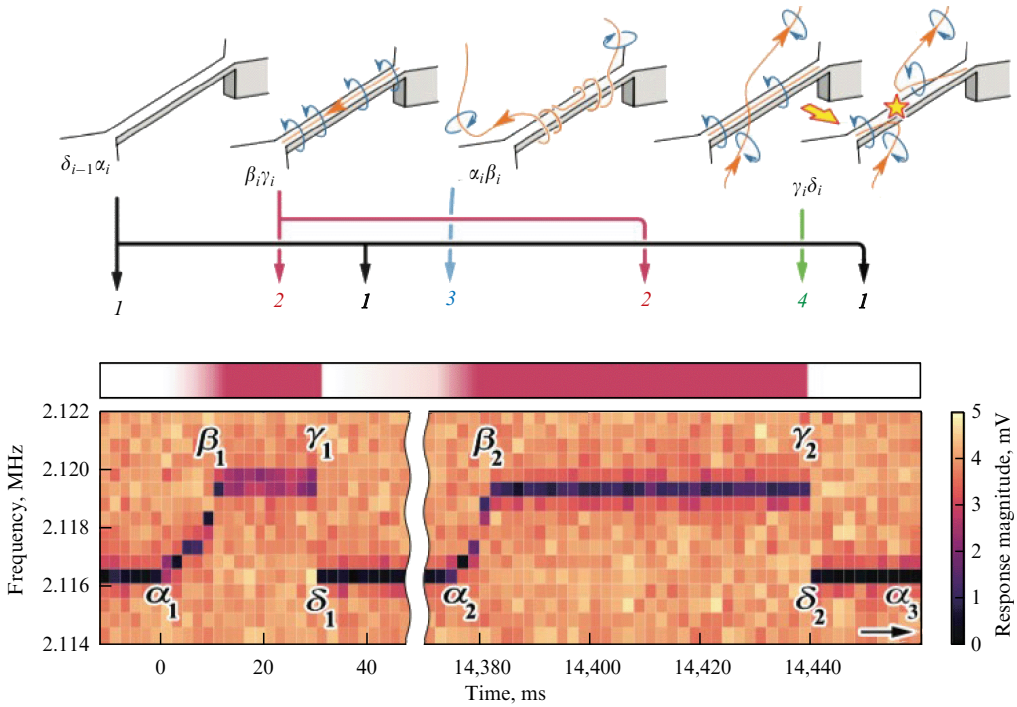

Figure 26. Time dependence of NEMS response to the capture of a vortex by a resonating nanobeam. Greek letters denote the times of change of the state of the resonator: state *1* — resonator is free of vortices, *2* — capture of the vortex by the resonator, *3* — vortex is captured by the resonator, *4* — extrication of the resonator from the vortex. Before time α_1, beam is in a vortex-free state. Between α_1 and β_1, the vortex interacting with the beam gradually increases the frequency of the beam by 3 kHz, and finally is captured along the entire length of the beam at point β_1. From β_1 to γ_1 the resonance is stable for 20 ms. Captured vortex interacts with a nearby vortex and at the point γ_1/δ_1 the system returns to the free state via reconnection of the trapped and attracted vortices. After 14.35 s, a second event occurs at the point α_2 with similar characteristics. Diagrams along the top of the figure depict the general processes that may be involved, although the exact details of capture and release mechanisms are not fully understood [184].

vortices pinned on the oscillator. For rough surfaces, such as quartz tuning forks or oscillating grids, there are many more opportunities for vortex engagement, which affects the existence of the TI regime with a subsequent transition to the TII regime of developed turbulence. After the transition of the tuning fork to the regime of quantum turbulence, some of the vortices after the completion of generation remain on the oscillator, and the drag coefficient of the oscillator increases in this case. The transition to the turbulent state will occur taking into account a new, denser system of pinned vortices at subsequent sweeps of the driving force.

For the sensitivity of all the above-described resonant systems as detectors of quantum turbulence, the mass of the detector itself and its area on which vortices can be pinned are fundamental. In this regard, the most sensitive one is NEMS, which is shown in Fig. 11c [121, 184]. Compared to other detecting systems, the mass of the working element (oscillating beam) is several orders of magnitude lighter, which apparently makes it possible to detect the pinning of individual vortices. At least, the response of the NEMS resonator during the generation of vortices in the surrounding space is always the same, and when a vortex is attached, the resonance frequency increases by 3 kHz (Fig. 26).

Let us pay attention to the characteristic response times of the detector to the arrival of the vortices. At a speed of movement of the prongs of the quartz tuning fork, starting from 73 mm s^{-1}, the NEMS resonator begins to detect the arrival of vortices, while the waiting time for the detector to operate is in the range from 40 to 1000 s. The probability density function of the waiting time between events $t_{\delta\alpha}$ for equal velocities of the quartz tuning fork (i.e., for the same vortex flow into the surrounding space) is described by an exponential of the form $P \propto \exp(-t_{\delta\alpha}/\tau)$. The characteristic vortex registration times τ varied from hundreds of seconds for 74 mm s^{-1} to $\tau \approx 7$ s for 90 mm s^{-1}. It should be noted that the transition of a quartz tuning fork from laminar motion ($F \sim v$) to turbulent motion ($F \sim v^2$) occurs at lower velocities ($\sim$ 65 mm s^{-1}), but registration of vortices under such excitations has not been experimentally observed and, most likely, the time constant for such a flow of vortices from the generator is much more than hundreds of seconds.

The turn-on times of the NEMS detector for all investigated modes ranged from fractions of a second to tens of minutes, which is apparently due to the need to pin the contact of a vortex of a suitable size on the surface of the NEMS resonator beam at the correct angle. However, the process of freeing the beam from the adhering vortex took place over times $t_{\alpha\gamma} = t_\alpha - t_\gamma$; much shorter, on the order of a few or ten milliseconds. From experiments on the visual behavior of vortices during reconnection [155, 185] and modeling the interaction of quantized vortices [186], the time characteristics of the interaction of vortices $t_{\alpha\gamma}$ during reconnection and the intervortex distance l RC are related as $l = A\sqrt{\kappa t_{\alpha\gamma}}$, where A is a value of the order of unity [155]. If we now assume that the characteristic time for an arbitrary vortex to stop a vortex 'adhered' to the resonator beam is $t_{\alpha\gamma} \approx 3-100$, then from $t_{\alpha\gamma} \approx 3-100$ ms follows a distance between vortices in a vortex tangle near the detector of 70–200 μm ($\mathcal{L} \sim 0.2 - 2 \times 10^4$ cm^{-2}), which is quite plausible.

A number of observations of the detection of vortices at macroscopic distances were made at temperatures above 1.2 K. At nonzero temperatures, when there is mutual friction between the normal and superfluid components, dissipation occurs, which reduces the diameter of the vortex

ring during its motion, and the ring will disappear after passing a certain distance. The rate of change of the vortex ring radius is defined as [8, 187, 188]

$$\dot{R} = -\alpha v(R)\,.$$

The vortex lifetime can be estimated as $\tau = R_0/(2\alpha v_0)$, where α is the coefficient of mutual friction between the normal and superfluid components of superfluid helium. The range of the ring before it disappears is given by [160]

$$l_\mathrm{b} = \int_0^\tau v\big(R(t)\big)\,\mathrm{d}t = \int_{R_0}^{\xi} v(R)\,\frac{\mathrm{d}t}{\mathrm{d}R}\,\mathrm{d}R = \frac{1}{\alpha}\,(R_0 - \xi)\,,$$

where ξ is the minimum size of the vortex of the order of the vortex core r_c; taking into account the smallness of the vortex core radius in comparison with the initial vortex radius, we finally get $l_\mathrm{b} = R_0/\alpha$. Therefore, for sufficiently strong dissipative processes in superfluid helium, the detection of vortices at a distance D is possible only for vortices with sizes larger than R_0, determined by the relation $2R_0 > 2\alpha D$.

In the Ueno group's work with superconducting wire resonators, a number of measurements on the detection of propagating vortices were carried out at high temperatures, which imposed certain restrictions on the size of the detected vortices that could reach the detector. Thus, the disappearance of a vortex with an initial radius of 18 μm will occur in 41 ms, and the distance traveled by it before disappearing is about 0.5 mm [189]. In [119], there are two detectors, one of which was placed in the direction of motion of the generator wire, and the other in the perpendicular direction (Fig. 11a). In this work, an anisotropy in the detection of vortices was shown. Taking into account the high temperature of superfluid helium in the experiment, the detector registered vortices with an initial diameter greater than 38 μm, which is comparable to the amplitude of the generator oscillations. If such a large vortex is formed and stretched by the motion of the wire, then the resulting vortex ring is likely to move perpendicular to the direction of the wire's path. In experiments, it was found that the detection of vortices occurs more often in the perpendicular direction than in the parallel direction. If we describe the probability of waiting for the operation of the detector $1 - P$ at time t after the generator is turned on, then the experimental observations are described by the relation

$$1 - P = \exp\left(-\frac{t - t_0}{t_1}\right),$$

where t_0 is the time of passage of the distance to the detector by the vortex, and t_1 is the average response time of the detector. For the direction of movement of the oscillation of the generator wire, the response time of the detector is $t_1 = 11$ s, while, for the perpendicular direction, $t_1 = 0.007$ s at a generation power of 500 pW. These measurements showed that the large vortex rings recorded in the experiment are emitted and move anisotropically, and they are detected in much greater numbers in the direction perpendicular to the motion of the generator wire.

Thus, by now it has been experimentally shown using the detection of vortices that vortices propagating over macroscopic distances are formed during quantum turbulence. At zero temperature, propagation distances are limited by the size of the cell. At temperatures above 0.3 K, the sizes of vortices decrease as they move due to interaction with excitations in a superfluid liquid — phonons and rotons. A similar anisotropic behavior of expanding vortex loops, albeit at zero temperature, was made in simulated experiments in [190]. It was shown that, when vortices are generated in an elongated volume of a parallelepiped, the probability of vortex diffusion in the direction perpendicular to the elongated direction of the source is much higher and the sizes of vortices in this direction are significantly larger, which also means that for the case of nonzero temperature there is a higher probability of registering vortices in this direction.

In Section 15, we estimate the number of vortices generated during the oscillation of resonators from the energy parameters of the oscillators and the change in their frequency during the detection of vortices.

15. Number of vortices generated in the process of oscillations

When discussing the problems of quantum turbulence, the question arises: how many vortices are created during the generation of a turbulent state at different velocities of an oscillating body? As experiments on the generation of quantum turbulence have shown, initially oscillating bodies move laminarly and only then, after exceeding the critical speed, do they begin to give rise to vortices that propagate through the space of the device at 'zero' temperature. As noted in Section 13, the transition from laminar motion to developed turbulence occurs in at least two stages, which differ, among other things, in the effect on the detector [65, 83, 124, 182].

One can calculate the energy transferred to the vortex system and estimate the number of vortices generated in the process of oscillations. This energy is the difference between the extrapolation of the linear dependence for laminar motion $F \sim V$ and the experimentally observed value $F(V)$. If we now estimate the power transferred to the system for one oscillation of an oscillating body, we can estimate the length of the vortex line generated in one period of oscillations ($E = \pi F_0 V_0/\omega$, where F_0 and V_0 are the force and velocity amplitudes, respectively) and compare it with the amplitude of oscillations in such a process.

For most oscillators, this power can be defined as the power of electrical losses of the external circuit: the speed of movement is determined by the bias current J for the capacitor in the case of a quartz tuning fork, a levitating sphere or an oscillating grid, and the voltage U is the magnitude of the external force through the appropriate coefficients. The energy of the external circuit in this case is not only transferred to the laminar motion but is also used to increase the length of the vortex system. In this case, the temperature of superfluid helium and the processes of energy dissipation of vortices after their creation is of little consequence — the energy of external excitation was transferred to the vortex system, and this power will be equal to $W = U^*(J_\mathrm{lin} - J)$, where J_lin is the linear extrapolation of current (velocity) dependence, corresponding to laminar motion of the oscillator. It is quite reasonable to assume that the distance between the vortices is in the range $l \sim 1$–100 μm ($\mathcal{L} \sim 10^4$–10^8 cm^{-2}), and then the energy of a unit length of the vortex (as the kinetic energy of the superfluid component) is determined as $E_\mathrm{L} \sim (1.0\text{–}1.4)\times 10^{-18}$ J μm.

When the levitating sphere oscillates [114] with diameter $d = 248$ μm (Fig. 22a), the difference between the continuation of the laminar velocity and the transition to turbulence is $\Delta v \approx 1$ cm s^{-1} at $F \sim 60$ pN, the power loss for the creation of vortices $W \approx 0.6$ pW, and for one half-cycle ($f = 114$ Hz) the length of the vortices increases by $\Delta L \sim 2000$ μm. An oscillation speed of 2 cm s^{-1} corresponds to an oscillation amplitude of $A = 28$ μm, which makes it possible to estimate $\Delta L_2/A \sim 80$ and $\Delta L_2/d \sim 9$.

Similarly, it is possible to estimate the number of generated vortices for a quartz tuning fork, taking into account the onset of the transition for different turbulence regimes: TI ($V_{cr1} \approx 0.5$ cm s^{-1}) and TII ($V_{cr2} \approx 15$ cm s^{-1}). For these velocities, with the oscillation frequency of such an oscillator at $f = 32$ kHz, the amplitudes will be $A_1 \approx 25$ nm and $A_2 \approx 700$ nm. The applied forces calculated from the calibration for these two cases will be 2 nN and 50 nN, and the energy transferred to the vortex system for one oscillation will be $E_1 = 5 \times 10^{-18}$ J and $E_2 = 3.5 \times 10^{-14}$ J. The vortex system for one oscillation will receive an increment in $\Delta L_1 \approx 4$ μm and $\Delta L_2 \approx 3 \times 10^4$ μm, which significantly exceeds the oscillation amplitude for these conditions in $\Delta L_1/A_1 \sim 160$ and $\Delta L_2/A_2 \sim 4.3 \times 10^4$. The dimensions of the quartz tuning fork prongs in these experiments were 3.676 mm long, 256 μm thick, and 616 μm wide. The gap between the prongs was 260 μm.

For a superconducting wire [133], the characteristic resonator values were: wire diameter $d = 2.5$ μm, wire arc radius $R \approx 0.5$ mm, oscillation frequency $f \approx 3.8$ kHz, $V_{cr2} \approx 7$ cm s^{-1}, $F \sim 120$ pN, oscillation amplitude $A \approx 3$ μm, transmitted energy at a half a period of oscillation $E \approx 3.6 \times 10^{-16}$ J. The addition of the length of the vortex system for one half-period of oscillation was $\Delta L_2 \sim 300$ μm and the ratio $\Delta L_2/A \sim 100$.

From the above estimation for various oscillating objects (levitating sphere, quartz tuning fork, superconducting arc) it follows that the increase in the length of the vortex system is much greater than the oscillation amplitude.

Estimates of the increase in the vortex system made for a MEMS resonator [124] with the dimensions of an oscillating plate 125×125 μm at a distance $h = 2$ μm from the substrate showed values closer to the oscillation amplitude. Here, the elongation of the vortex system was comparable to the amplitude of the oscillations. The oscillation frequency was $f = 23$ kHz. For the first critical speed $V_{cr1} = 0.5$ cm s^{-1} of the beginning of vortex generation, applied force $F_1 \sim 7$ pN, amplitude $A_1 \approx 35$ nm, energy $E_1 \approx 0.25 \times 10^{-18}$ J transferred to the vortex system increases the length of the vortex system in one half-cycle $\Delta L_1 \sim 0.2$ μm, which exceeds the oscillation amplitude $\Delta L_1/A_1 \sim 6$. Similar estimates for speed $V_{cr2} = 14.0$ cm s^{-1}, at which the behavior of the MEMS resonator changes, give: $F_2 \sim 30$ pN, $A_2 \approx 900$ nm, $E_2 \approx 27 \times 10^{-18}$ J, and the gain of the vortex system $\Delta L_2 \sim 22$ μm ($\Delta L_2/A_2 \sim 25$).

In a number of studies, the density of pinned vortices was estimated as a change in the detector frequency due to an increase in the rigidity of the system through the attached vortices. As experiments have shown for all vortex detectors based on high-Q oscillators, the response to the inclusion of quantum turbulence led to an increase in the resonant frequency. We noted that to date the question of vortices as an added mass has not been fully elucidated. In a number of papers, the pinning of additional vortices is considered an additional force due to an increase or decrease in the length of the vortex line during motion of the oscillator. In this regard, the results with a NEMS oscillator were significative. According to the authors [184], the addition of just one vortex always led to the same increase in the oscillation frequency by 3 kHz (Fig. 26).

The change in the resonator frequency during pinning of vortices (or one vortex) on it can be used to estimate the number of vortices. In [184], estimates of the elastic properties of a resonator nanobeam based on natural vibrations of a bar clamped on both sides [191] give the value $T_0 \approx 5.6$ μN for the tension of the rod as a string. Accounting for the added mass of superfluid helium and additional acoustic damping, as discussed in Sections 5, 8, gives the oscillation frequency $f \approx 2.116$ MHz. The main change in the NEMS oscillation frequency is related to the coupling of the vortex to the nanobeam, which can be calculated by the imaging method as the interaction between the vortex on the nanobeam and the substrate. The distance between the nanobeam and the substrate is $d \approx 1$ μm, and it can be represented that the vortex interacts with the image — with a parallel vortex located at distance $2d$ from it. An estimate of the attractive force in this case gives $F \sim 8$ pN. This force leads to a deflection of the nanobeam, which changes the oscillation frequency upward by ~ 1 kHz, which coincides in order of magnitude with the observed value. The Magnus force during the oscillation of the vortex attached to the oscillator will determine the addition to the nanobeam tension, but this shift is of the order of 10 Hz.

The additional tension of the pinned vortices explains the stepwise increase in the oscillation frequency of the wire resonator [178], which acts as a turbulence detector. The change in the oscillation frequency of this oscillator occurs due to the appearance of an additional tension of the vortex cores connecting the oscillating wire with the walls of the cell. Estimates [167] of the tension of the vortices due to the oscillation of the wire under the assumption that the vortex connects the tip of the detecting wire and the nearest wall of the ampoule give, for the real dimensions of the ampoule, a change in the oscillation frequency of ~ 0.7 mHz per pinned vortex. The observed increase in the resonant frequency by 0.3 Hz may be explained as several hundred bridge vortex lines. With a wire resonator length of 1 mm, the distance between the pinned vortices should be on the order of several μm.

From general considerations, it is clear that a change in the frequency of oscillations of resonators associated with the addition of vortices could be registered in the case of a small mass of an oscillating body, when a small change in the forces in the system due to interaction with vortices has a visible effect on the resonant properties. So, such frequency changes affect measurements with NEMS nanobeams ($m \sim 15$ pg) and superconducting wire ($m \sim 10$ ng). However, an increase in resonant frequencies was observed for much heavier quartz tuning forks ($m \sim 400$ μg) [182], which is not entirely clear. We mention that the mass of the oscillating grid [107] is the largest, taking into account the large size of the oscillating oscillator ($d \approx 10$ cm), and has the order of $m \sim 85$ mg, the levitating spheres having $m \sim 20$ mg [112]. The MEMS resonator turned out to be much lighter — $m \sim 0.3$ μg.

To estimate the increase in the attenuation of oscillations of the MEMS resonator during the detection of vortices, it was assumed in [124] that, when oscillating along the plane of the resonator plate, the vortices attached along the edge of the plate change their length due to the shift of the pinning point when the plate oscillates, $\delta l \sim A_2/2d$, where d are the

distances from the oscillator plate to the substrate. Then, to create additional damping of the oscillator when vortices are attached, it is necessary that the vortices radiate vortex loops due to reconnections and carry away additional energy from the oscillator. The number of such vortices to fulfill the damping conditions should be ~ 400, and when they are fixed along the perimeter of the oscillator plate, the distance between the pinned vortices will be about 1–10 μm.

Several conclusions can be drawn based on estimates of the creation and pinning of vortices in oscillating systems. First, the number of vortices varies depending on the prehistory; by slowly filling the cell, one can achieve the state of a vortex system in superfluid helium with the virtual absence of remanent vortices and vortices pinned on the oscillator (virgin state). In this case, the transition of the oscillator to the turbulent state can occur at significantly higher velocities of the oscillating element. The transition to turbulence leads to a sharp increase in the number of pinned vortices on the oscillator, which can be removed and the oscillator returned to the initial 'virgin' state only by special tricks. Second, the length of the vortex structures generated in one oscillation for all of the above resonators is significantly greater than the oscillation amplitude of these oscillators from tens (for MEMS oscillators) to tens of thousands (for quartz tuning forks). Third, the distance between the pinned vortices on any oscillator is of the order of 1–10 μm, which gives an estimate for the vortex density of $\mathcal{L} \sim 10^6 - 10^8$ cm^{-2}.

An estimation of the rates of vortex generation from 'zero' — vortex nucleation from a wall without a spin vortex — shows (Section 2, Fig. 1g) that vortex generation always occurs at significantly lower velocities. It is difficult to assume that a vortex pinned by two ends on an oscillator can launch a loop with a length greater than the amplitude of oscillations into superfluid helium in one half-period of oscillations. If we assume that the length of a pinned vortex grows by gradually increasing its length during successive oscillations of the oscillator, then the characteristic radius of the vortex loops cannot exceed the distance between the pinned vortices, i.e., 1–10 μm. However, observations of detection at nonzero temperatures, when vortices of small diameter disappear due to interaction with rotons and phonons in superfluid helium, showed in [119, 189] that the size of vortices reaching the detector at a distance of ~ 1 mm was initially significantly larger ($R > 30$ μm), for both the oscillation amplitude of the wire oscillator ($A \approx 3$ μm) and the diameter of this wire ($d = 2.5$ μm).

The mechanism of quantum turbulence generation can be represented as the formation of vortex loops from many vortices pinned between the oscillator and the ampoule walls. The formation of kinks during the motion of vortex pinning points, self-intersection, and intersection with neighboring vortices, and reconnection processes lead not only to a decrease in the size of vortex loops near the source of vortices but also to their growth, which is observed in experiments. An increase in the size of single vortices at the boundary of the vortex generation zone was observed in computer simulations [190]. The transition to quantum turbulence during resonator oscillations is accompanied by an increase in the interaction of generated vortices with their source, i.e., with an oscillator. This interaction leads to an increase in the number of vortices pinning on the oscillator, which was described above as a transition to a regular state from a virgin one.

An increase in the damping of independent oscillations upon the transition of a quartz tuning fork to the generation of vortices was experimentally observed in Ref. [192]. For the experiments, a quartz tuning fork was made with a specially chosen orientation of the crystal axes, which made it possible to create two independent vibration modes from the same electrodes — bending and torsion. It turned out that, during the transition of the bending mode to the generation of vortices and transition to quantum turbulence, the torsion mode begins to experience additional damping, the magnitude of which depends on the intensity of the generation of vortices. This indicates that, during the generation of a turbulent state in superfluid helium, some of the generated vortices are attached to the surface of a quartz tuning fork, which changes the quality factor of torsion oscillations, as in the case of a tuning fork when it detects vortices reaching its surface [182].

16. Conclusion

In this review of quantum turbulence, we mainly focus on recent work on the generation of vortices using oscillators, which allow measurements to be executed at very low temperatures under conditions of freezing of thermal excitations in superfluid helium. The features of superfluid helium, namely, the quantization of the flow of the superfluid component around vortices, the definite position of the vortex core, and the purity of the liquid (the amount of impurity in liquid helium can be reduced to less than 10^{-11}% [193]), make it a model medium for studying the formation and decay of turbulent systems. The behavior of quantum turbulence is determined by two parameters — the superfluid Reynolds number $\mathrm{Re}_s = VD/\kappa$, where V is the velocity of the fluid or body relative to the fluid, D is the size of the system, and κ is the circulation quantum, and the ratio of dissipative to inertial processes in superfluid helium $q = \alpha/(1 - \alpha')$, where the dimensionless parameters α' and α determine the reactive and dissipative forces acting on the vortex when it moves relative to the normal component.

The state of quantum turbulence, the rate of generation of vortices in the counterflow of the normal and superfluid components, and the decay of the vortex system are quite well quantitatively described by the phenomenological Vinen's equation. An increase in the density of vortices at a stationary heat flux according to Vinen's equation is possible only in the presence of residual vortices in superfluid helium (remanent vorticity). The presence of a vortex system can be detected by the absorption of second-sound waves, which is most often used at temperatures above 1.2 K, as well as by the response of high-Q resonators to their interaction with vortices.

During oscillatory processes around moving bodies, when critical velocities are exceeded in superfluid helium, quantized vortices are generated. It is this technique that is used at low temperatures (below 0.1 K), when intrinsic excitations in superfluid helium (rotons and phonons) can be ignored. Vibrating grids, levitating spheres, superconducting wires, and quartz tuning forks are currently used as oscillatory systems. Recently, micro- and nano-electromechanical systems (MEMS and NEMS) have begun to be used as small-sized resonators.

The transition from the laminar to the turbulent state occurs, judging by the experimental data, in at least two stages. At the first stage, *single vortex loops* are formed by elongation of the residual vortices and their reconnection, i.e., by crossing with themselves and with nearby vortices during

the motion of the superfluid component either due to the counterflow of the normal and superfluid components during heat release or during the motion of oscillating objects with pinned vortices. With a stronger counterflow of the normal and superfluid components or the oscillation velocity of oscillators in superfluid helium, a developed turbulent state is formed in which the number of vortices in the space surrounding the oscillator sharply increases. It may screen the flow of vortex flux from the oscillator, and the number of vortices pinned on the oscillator increases — there is a transition from the virgin state to the regular state. Such a two-stage transition was registered by the change in the temperature gradient during heat release, by the behavior of the resistance coefficient of oscillating resonators to a change in external excitation, and by the response of high-Q resonators, as vortex detectors, when turbulent states are excited at macroscopic distances from the source of vortices.

The oscillatory processes of high-quality resonant systems used to generate vortices in superfluid helium are accompanied by the emission of sound waves, which can be the dominant oscillator in energy losses at vibration frequencies above 100 kHz. The critical velocities of oscillatory processes that bring a superfluid liquid into a turbulent state are proportional to the root dependence on the oscillation frequency.

When vortex turbulence is generated by oscillating bodies, the increment in the length of vortex lines can be estimated as an excess of energy transfer compared to laminar motion. Estimates show that the increase in the length of the vortex system during the half-period of oscillations of generating oscillators is tens, hundreds, or even thousands of times greater than the amplitude of these oscillations. This indicates that the increase in the density of vortices in superfluid helium during turbulence is a collective process involving a large number of vortices pinned on the oscillator. A small number of vortices pinned on the oscillator and its smooth surface led to a significant increase in the critical velocities of the transition to turbulence, a substantial hysteresis with sweeping up and down excitations of the oscillator. The departure of vortex loops from the oscillator is determined by the processes of reconnection of pinned vortices both on themselves and on neighboring vortices, the density of which on the vortex generator can reach values of the order of $10^6 - 10^8$ cm^{-2}.

Qualitative analysis makes it possible to estimate the effective viscosity of a superfluid liquid in the presence of a vortex structure. With such an estimate, it turns out that the effective viscosity for quantum turbulence will be of the order of the circulation quantum,

$$\nu' = \left(\frac{\beta}{C_{\mathrm{K}}}\right)^{3/2} \kappa ,$$

where the constants in parentheses are of the order of unity.

The main mechanism of energy dissipation of the vortex system at low temperatures is apparently the Kelvin waves that appear during reconnection as the movement of sharp kinks, which is confirmed by visual observations. The motion of Kelvin waves along the core of the vortex is accompanied by the emission of phonons and the loss of energy by the vortex loop.

The author is grateful to P V E McClintock, Deepak Garg, O Kolosov, S Kafanov, I Aleskerov, and A Esina, with whom it was a pleasure to work and with whom many of the studies presented in the review were co-authored. The author is grateful to A A Levchenko, L P Mezhov-Deglin, L Skrbek, W F Vinen, V V Lebedev, E A Kuznetsov, I V Kolokolov, S K Nemirovsky, and L P Kondaurova for their numerous and useful discussions of quantum turbulence problems. The work was supported by RFBR grant no. 20-12-50135, 'Expansion'.

References

1. Efimov V B *Phys. Usp.* **61** 929 (2018); *Usp. Fiz. Nauk* **188** 1025 (2018)
2. Donnelly R J, Swanson C E *J. Fluid Mech.* **173** 387 (1986)
3. Niemetz M, Kerscher H, Schoepe W, in *Quantized Vortex Dynamics and Superfluid Turbulence* (Eds C F Barenghi, R J Donnelly, W F Vinen) (Berlin: Springer, 2001) p. 87
4. Tsubota M (Ed.) *Quantum Turbulence* (Progress in Low Temperature Physics, Vol. 16) (Amsterdam: Elsevier Science, 2008)
5. Vinen W F, Niemela J J *J. Low Temp. Phys.* **128** 167 (2002)
6. Skrbek L *J. Phys. Conf. Ser.* **318** 012004 (2011)
7. Barenghi C F, Skrbek L, Sreenivasan K R *Proc. Natl. Acad. Sci. USA* **111** (Suppl. 1) 4647 (2014)
8. Donnelly R J *Quantized Vortices in Helium II* (Cambridge: Cambridge Univ. Press, 1991)
9. Kondaurova L P, Andryushchenko V A *Low Temp. Phys.* **47** 740 (2021); *Fiz. Nizk. Temp.* **47** 804 (2021)
10. Kapitsa P L *Dokl. Akad. Nauk SSSR* **18** (1) 21 (1938)
11. Lifshits E M *Usp. Fiz. Nauk* **34** 512 (1948)
12. Landau L D *Zh. Eksp. Teor. Fiz.* **11** 592 (1941)
13. Landau L D *Zh. Eksp. Teor. Fiz.* **14** 112 (1944)
14. Craig P P, Pellam J R *Phys. Rev.* **108** 1109 (1957)
15. Allen J F, Misener A D *Proc. R. Soc. A* **172** 467 (1939)
16. Atkins K R *Adv. Phys.* **1** 169 (1952)
17. Nemirovskii S K *Phys. Rep.* **524** 85 (2013)
18. Barenghi C F, Donnelly R J, Vinen W F *J. Low Temp. Phys.* **52** 189 (1983)
19. Finne A P et al. *Rep. Prog. Phys.* **69** 3157 (2006)
20. Vinen W F *Proc. R. Soc. A* **260** 218 (1961)
21. Whitmore S C, Zimmermann W *Phys. Rev. Lett.* **15** 389 (1965)
22. Rayfield G W, Reif F *Phys. Rev.* **136** A1194 (1964)
23. Gamota G *J. Phys. Colloq.* **31** C3-39 (1970)
24. Barenghi C F et al. *Phys. Fluids* **9** 2631 (1997)
25. Koplik J, Levine H *Phys. Rev. Lett.* **71** 1375 (1993)
26. Vinen W F, Skrbeck L *Proc. Natl. Acad. Sci. USA* **111** (Suppl. 1) 4699 (2014)
27. Zurek W H *Nature* **317** 505 (1985)
28. Copeland E J, Kibble T W B, Steer D A *Phys. Rev. D* **58** 043508 (1998)
29. Kibble W B *J. Phys. A* **9** 1387 (1976)
30. Efimov V B et al. *Phys. Rev. E* **74** 056305 (2006)
31. Tilley D R, Tilley J *Superfluidity and Superconductivity* (New York: Wiley, 1974); Translated into Russian: *Sverkhtekuchest' i Sverkhprovodimost'* (Moscow: Mir, 1977)
32. Tkachenko V K *Sov. Phys. JETP* **22** 1282 (1966); *Zh. Eksp. Teor. Fiz.* **49** 1875 (1965)
33. Tkachenko V K *Sov. Phys. JETP* **23** 1049 (1966); *Zh. Eksp. Teor. Fiz.* **50** 1573 (1966)
34. Tkachenko V K *Sov. Phys. JETP* **29** 945 (1969); *Zh. Eksp. Teor. Fiz.* **56** 1763 (1969)
35. Tsakadze S J *Fiz. Nizk. Temp.* **4** (2) 148 (1978)
36. Gordon M J V, Williams G A, Packard R E *J. Phys. Colloq.* **39** C6-17 (1978)
37. Yarmchuk E J, Gordon M J V, Packard R E *Phys. Rev. Lett.* **43** 214 (1979)
38. Walmsley P M et al. *Phys. Rev. Lett.* **99** 265302 (2007)
39. Tsubota M et al. *Phys. Rev. B* **69** 134515 (2004)
40. Smith M R et al. *Phys. Rev. Lett.* **71** 2583 (1993)
41. Stalp S R, Skrbek L, Donnelly R J *Phys. Rev. Lett.* **82** 4831 (1999)
42. Skrbek L, Niemela J J, Donnelly R J *Phys. Rev. Lett.* **85** 2973 (2000)
43. Maurer J, Tabeling P *Europhys. Lett.* **43** 29 (1998)
44. Volovik G E *JETP Lett.* **78** 533 (2003); *Pis'ma Zh. Eksp. Teor. Fiz.* **78** 1021 (2003)

45. Hall H E, in *Liquid Helium, Proc. of the Intern. School of Physics* "*Enrico Fermi*", *Course XXI* (Ed. G Carreri) (New York: Academic Press, 1963)
46. Sonin E B *Rev. Mod. Phys.* **59** 87 (1987)
47. Volovik G E *J. Low Temp. Phys.* **136** 309 (2004); cond-mat/0402035
48. Skrbek L *JETP Lett.* **80** 474 (2004); *Pis'ma Zh. Eksp. Teor. Fiz.* **80** 541 (2003)
49. Baehr M L, Opatowsky L B, Tough J T *Phys. Rev. Lett.* **51** 2295 (1983)
50. Ladner D R, Childers R K, Tough J T *Phys. Rev. B* **13** 2918 (1976)
51. Chase C E *Phys. Rev.* **127** 361 (1962)
52. Salort J et al. *J. Phys. Conf. Ser.* **318** 042014 (2011)
53. Donnelly R J, Barenghi C F *J. Phys. Chem. Ref. Data* **27** 1217 (1998)
54. Baggaley A W et al. *Phys. Rev. B* **86** 104501 (2012)
55. Walmsley P M, Golov A I *Phys. Rev. Lett.* **100** 245301 (2008)
56. Skrbek L, Sreenivasan K R, in *Ten Chapters in Turbulence* (Eds P A Davidson, Y Kaneda, K R Sreenivasan) (New York: Cambridge Univ. Press, 2013)
57. Vinen W F *Proc. R. Soc. Lond. A* **240** 114 (1957)
58. Baggaley A W, Barenghi C F, Sergeev Y A *Phys. Rev. B* **85** 060501 (2012)
59. Finne A P et al. *Nature* **424** 1022 (2003)
60. Vinen W F *Proc. R. Soc. Lond. A* **240** 128 (1957)
61. Vinen W F *Proc. R. Soc. Lond. A* **242** 493 (1957)
62. Vinen W F *Proc. R. Soc. Lond. A* **243** 400 (1958)
63. Hall H E, Vinen W F *Proc. R. Soc. Lond. A* **238** 215 (1956)
64. Monin A S, Yaglom A M *Statistical Fluid Dynamics*; *Mechanics of Turbulence* Vol. 2 (Cambridge, MA: MIT Press, 1975); Translated from Russian: *Statisticheskaya Gidromekhanika* Vol. 2 (Moscow: Nauka, 1967)
65. Garg D et al. *Phys. Rev. B* **85** 144518 (2012)
66. Donnelly R J *Phys. Today* **62** (10) 34 (2009)
67. Efimov V B et al. *J. Low Temp. Phys.* **156** 95 (2009)
68. Ganshin A N et al. *New J. Phys.* **12** 083047 (2010)
69. Snyder H A, Putney Z *Phys. Rev.* **150** 110 (1966)
70. Mathieu P, Placais B, Simon Y *Phys. Rev. B* **29** 2489 (1984)
71. Giltrow M et al. *Meas. Sci. Technol.* **14** N69 (2003)
72. Varga E et al. *J. Low Temp. Phys.* **197** (3/4) 130 (2019)
73. Jackson M J *J. Low Temp. Phys.* **183** 208 (2016)
74. Ferrell R A *Phys. Rev.* **108** 167 (1957)
75. Atkins K R *Phys. Rev.* **116** 1339 (1959)
76. Marakov A et al. *Phys. Rev. B* **91** 094503 (2015)
77. Gao J et al. *JETP Lett.* **103** 648 (2016); *Pis'ma Zh. Eksp. Teor. Fiz.* **103** 732 (2016)
78. Chase C E *Phys. Rev.* **131** 1898 (1963)
79. Arp V *Cryogenics* **10** 96 (1970)
80. Gorter C J, Mellink J H *Physica* **15** 285 (1949)
81. Schwarz K W *Phys. Rev. B* **18** 245 (1978)
82. Van Sciver S W *Cryogenics* **18** 521 (1978)
83. Brewer D F, Edwards D O *Philos. Mag.* **7** 721 (1962)
84. Iznankin A Yu, Mezhov-Deglin L P *Sov. Phys. JETP* **84** 1378 (1983); *Zh. Eksp. Teor Fiz.* **103** 732 (2016)
85. Efimov V B et al. *Low Temp. Phys.* **24** 81 (1998); *Fiz. Nizk. Temp.* **24** 116 (1998)
86. Nemirovskii S K, Tsoi A N *Cryogenics* **29** 985 (1989)
87. Hall H E *Adv. Phys.* **9** 89 (1960)
88. Kondaurova L, Efimov V, Tsoi A *J. Low Temp. Phys.* **187** 80 (2017)
89. Tsoi A N, Lutset M O *J. Eng. Phys.* **51** 749 (1986); *Inzh.-Fiz. Zh.* **51** (1) 5 (1985)
90. Peshkov V P, Tkachenko V K *Sov. Phys. JETP* **14** 1019 (1962); *Zh. Eksp. Teor. Fiz.* **41** 1427 (1961)
91. Awschalom D D, Milliken F P, Schwarz K W *Phys. Rev. Lett.* **53** 1372 (1984)
92. Tough J T, in *Progress in Low Temperature Physics* Vol. 8 (Ed. D F Brewer) (Amsterdam: North-Holland, 1982) p. 133
93. Brewer D F, Edwards D O *Philos. Mag.* **6** 1173 (1961)
94. Adachi H, Fyjiyama S, Tsubota M *Phys. Rev. B* **81** 104511 (2010)
95. Melotte D J, Barenghi C F *Phys. Rev. Lett.* **80** 4181 (1998)
96. Chagovets T V, Skrbek L *Phys. Rev. Lett.* **100** 215302 (2008)
97. Skrbek L, Vinen W F, in *Quantum Turbulence* (Progress in Low Temperature Physics, Vol. 16, Eds M Tsubota, W P Halperin) (Amsterdam: Elsevier, 2009) p. 195
98. Vinen W F, Skrbek L *Proc. Natl. Acad. Sci. USA* **111** (Suppl. 1) 4699 (2014)
99. Tatsuno M, Bearman P *J. Fluid Mech.* **211** 157 (1990)
100. Uzunoğlu B, Tan M, Price W G *Int. J. Numer. Meth. Eng.* **50** 2317 (2001)
101. Batchelor G K *An Introduction to Fluid Dynamics* (Cambridge: Cambridge Univ. Press, 1967)
102. Smith M R et al. *Phys. Rev. Lett.* **71** 2583 (1993)
103. Yang J, Ihas G G *J. Phys. Conf. Ser.* **969** 012004 (2018)
104. Stalp S R et al. *Phys. Fluids* **14** 1377 (2002)
105. Niemela J J, Sreenivasan K R, Donnelly R J *J. Low Temp. Phys.* **138** 537 (2005)
106. Rusaouen E et al. *Phys. Fluids* **29** 105108 (2017)
107. Nichol H A et al. *Phys. Rev. E* **70** 056307 (2004)
108. Vinen W F, Skrbek L, Nichol H A *J. Low Temp. Phys.* **135** 423 (2004)
109. Nichol H A "Experimental investigation of the macroscopic flow of helium II at mK temperatures", PhD Thesis (Lancaster: Lancaster Univ., 2003)
110. Charalambous D et al. *Phys. Rev. E* **74** 036307 (2006)
111. Efimov V B et al. *J. Low Temp. Phys.* **158** 462 (2010)
112. Jäger J, Schuderer B, Schoepe W *Phys. Rev. Lett.* **74** 566 (1995)
113. Schoepe W *Phys. Rev. Lett.* **92** 095301 (2004)
114. Schoepe W *J. Low Temp. Phys.* **161** 526 (2010)
115. Niemetz M, Kerscher H, Schoepe W *J. Low Temp. Phys.* **126** 287 (2002)
116. Blaauwgeers R et al. *J. Low Temp. Phys.* **146** 537 (2007)
117. Fisher S N et al. *Phys. Rev. Lett.* **86** 244 (2001)
118. Nago Y et al. *Phys. Rev. B* **82** 224511 (2010)
119. Yano H et al. *J. Low Temp. Phys.* **187** 515 (2017)
120. González M et al. *Rev. Sci. Instrum.* **84** 025003 (2013)
121. Guénault A M et al. *Phys. Rev. B* **100** 020506 (2019)
122. Barquist C S et al. *J. Low Temp. Phys.* **183** 307 (2016)
123. Zheng P et al. *J. Low Temp. Phys.* **183** 313 (2016)
124. Barquist C S et al. *J. Low Temp. Phys.* **201** 4 (2020)
125. Koester D et al., PolyMUMPs Design Handbook (Durham, NC: MEMSCAP, 2005); http://www.memscap.com/products/mumps
126. Guthrie A et al. *Nat. Commun.* **12** 2645 (2021)
127. Guénault A M at al. *Phys. Rev. B* **101** 060503 (2020)
128. Ahlstrom S L et al. *Phys. Rev. B* **89** 014515 (2014)
129. Bradley D I et al. *Phys. Rev. B* **85** 014501 (2012)
130. Sheshin G et al. *Low Temp. Phys.* **39** 823 (2013); *Fiz. Nizk. Temp.* **39** 1062 (2013)
131. Schmoranzer D et al. *J. Low Temp. Phys.* **163** 317 (2011)
132. Bradley D I et al. *J. Low Temp. Phys.* **156** 116 (2009)
133. Yano H et al. *AIP Conf. Proc.* **850** 195 (2006)
134. Luzuriaga J *J. Low Temp. Phys.* **138** 267 (1997)
135. Bradley D I et al. *Phys. Rev. Lett.* **96** 035301 (2006)
136. Vinen W F *J. Low Temp. Phys.* **145** 7 (2006)
137. L'vov V, Nazarenko S, Skrbek L *J. Low Temp. Phys.* **145** 125 (2006)
138. Kozik E V, Svistunov B V *J. Low. Temp. Phys.* **156** 215 (2009)
139. Bradley D I et al. *Phys. Rev. Lett.* **101** 065302 (2008)
140. Roche P-E et al. *Europhys. Lett.* **77** 66002 (2007)
141. Sasa N et al. *Phys. Rev. B* **84** 054525 (2011)
142. Baggaley A W, Laurie J, Barenghi C F *Phys. Rev. Lett.* **109** 205304 (2012)
143. Kotsubo V, Swift G W *Phys. Rev. Lett.* **62** 2604 (1989)
144. Kotsubo V, Swift G W *J. Low Temp. Phys.* **78** 351 (1990)
145. Hänninen R, Schoepe W *J. Low Temp. Phys.* **164** 1 (2011)
146. Hänninen R, Schoepe W, arXiv:0801.2521
147. Hänninen R, Schoepe W *J. Low Temp. Phys.* **153** 189 (2008)
148. Hänninen R, Schoepe W *J. Low Temp. Phys.* **158** 410 (2010)
149. Vinen W F *Phys. Rev. B* **61** 1410 (2000)
150. Tsubota M, Araki T, Nemirovskii S K *Phys. Rev. B* **62** 11751 (2000)
151. Paoletti M S et al. *J. Phys. Soc. Jpn.* **77** 111007 (2008)
152. Meichle D P, Lathrop D P *Rev. Sci. Instrum.* **85** 073705 (2014)
153. Bewley G P, Sreenivasan K R, Lathrop D P *Exp. Fluids* **44** 887 (2008)
154. Fonda E et al. *Proc. Natl. Acad. Sci. USA* **111** (Suppl. 1) 4707 (2014)
155. Fonda E, Sreenivasan K R, Lathrop D P *Proc. Natl. Acad. Sci. USA* **116** 1924 (2019)
156. Howe M S *Acoustics of Fluid-Structure Interactions* (Cambridge: Cambridge Univ. Press, 1998)

157. Vinen W F *Phys. Rev. B* **64** 134520 (2001)
158. L'vov V S, Nazarenko S V, Rudenko O *Phys. Rev. B* **76** 024520 (2007)
159. Niemetz M, Schoepe W *J. Low Temp. Phys.* **135** 447 (2004)
160. Bradley D I et al. *J. Low Temp. Phys.* **138** 493 (2005)
161. Blažková M, Schmoranzer D, Skrbek L *Phys. Rev. E* **75** 025302 (2007)
162. Hashimoto N et al. *Phys. Rev. B* **76** 020504 (2007)
163. Yano H et al. *J. Low Temp. Phys.* **150** 410 (2008)
164. Garg D "Experimental investigation of quantized vortices using grid and quartz tuning forks in superfluid helium-4 in the zero temperature limit", PhD Thesis (Lancaster: Depart. of Physics, Lancaster Univ., 2010)
165. Blažková M et al. *J. Low Temp. Phys.* **148** 305 (2007)
166. Schoepe W, Hänninen R, Niemetz M *J. Low Temp. Phys.* **178** 383 (2015)
167. Hänninen R, Tsubota M, Vinen W F *Phys. Rev. B* **75** 064502 (2007)
168. Hall H *Phil. Trans. R. Soc.* **250** 359 (1957)
169. Kondaurova L P, Nemirovskii S K *Low Temp. Phys.* **37** 413 (2011); *Fiz. Nizk. Temp.* **37** 523 (2011)
170. Kondaurova L, Nemirovskii S K *Phys. Rev. B* **86** 134506 (2012)
171. Schwarz K W *Phys. Rev. B* **38** 2398 (1988)
172. Nakatsuji A, Tsubota M, Yano H *J. Low Temp. Phys.* **171** 519 (2013)
173. Barenghi C F, Hänninen R, Tsubota M *Phys. Rev. E* **74** 046303 (2006)
174. Nemirovskii S K *Phys. Rev. B* **81** 064512 (2010)
175. Popov V N *Sov. Phys. JETP* **37** 341 (1973); *Zh. Eksp. Teor. Fiz.* **64** 672 (1973)
176. Thouless D J, Anglin J R *Phys. Rev. Lett.* **99** 105301 (2007)
177. Duan J-M *Phys. Rev. B* **49** 12381 (1994)
178. Nago Y et al. *J. Low Temp. Phys.* **158** 443 (2010)
179. Yano H et al. *Phys. Rev. B* **81** 220507 (2010)
180. Kubo H et al. *J. Low Temp. Phys.* **171** 466 (2013)
181. Yano H et al. *J. Low Temp. Phys.* **156** 132 (2009)
182. Garg D et al. *Low Temp. Phys.* **38** 1026 (2012); *Fiz. Nizk. Temp.* **38** 1300 (2012)
183. Nago Y et al. *Phys. Rev. B* **87** 024511 (2013)
184. Guthrie A et al., arXiv:2007.04482
185. Bewley G et al. *Proc. Natl. Acad. Sci. USA* **105** 13707 (2008)
186. Galantucci L et al. *Proc. Natl. Acad. Sci. USA* **116** 12204 (2019)
187. Bewley G P *Cryogenics* **49** 549 (2009)
188. Bewley G P, Sreenivasan K R *J. Low Temp. Phys.* **156** 84 (2009)
189. Nago Y et al. *J. Low Temp. Phys.* **162** 322 (2011)
190. Bao M *Analysis and Design Principles of MEMS Devices* (Amsterdam: Elsevier Science, 2005)
191. Nakagawa T et al. *Phys. Rev. B* **101** 184515 (2020); arXiv:2002.05387v3
192. Guthrie A et al. *Appl. Phys. Lett.* **115** 113103 (2019)
193. Hendry P C, McClintock P V E *Cryogenics* **27** 131 (1987)